Comprehensive analysis of the transcription factor REST regulatory networks in IDH-mutant and IDH-wild type glioma

Malgorzata Perycz*[1,2], Michal J. Dabrowski*[2], Marta Jardanowska[2], Adria-Jaume Roura[1], Bartlomiej Gielniewski[1], Karolina Stepniak[1], Michał Dramiński[2], Bozena Kaminska[1], Bartosz Wojtas[1,3]#

[1] Laboratory of Molecular Neurobiology, Nencki Institute of Experimental Biology, Polish Academy of Sciences
[2] Computational Biology Group, Institute of Computer Science of the Polish Academy of Sciences, Warsaw, Poland
[3] Laboratory of Sequencing, Nencki Institute of Experimental Biology, Polish Academy of Sciences

* First author, shared
# Corresponding author

Graphical abstract

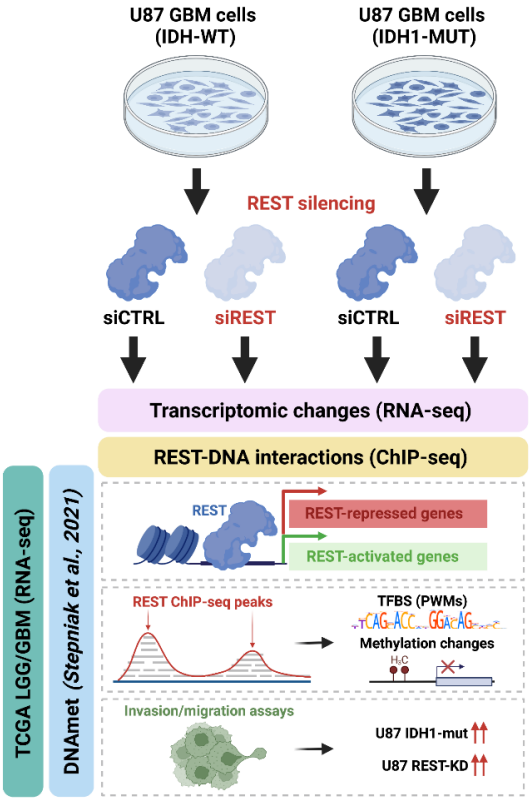

Summary (150 words)

REST acts as a transcriptional repressor of neuronal genes in non-neuronal cells but could be a transcriptional activator under certain conditions. REST was implicated in a blockage of cell differentiation and is an important oncogenic factor. As IDH mutations are oncogenic drivers in gliomas causing significant changes in the epigenome and blocking differentiation, we aimed at defining the role of REST in the IDH mutation-related phenotype in gliomas. We studied consequences of REST knockdown in IDH wild-type and mutant U87 cells. Chromatin immunoprecipitation followed by sequencing combined with transcription factor (TF) motif identification and transcriptome analyses revealed different patterns of REST binding and its proximal TF motifs in IDH wild-type and mutant U87 cells. Moreover, we identified putative targets of REST as related to ECM organization and cell differentiation. We demonstrate that the REST role in gliomas is dependent on IDH mutation status.

Keywords

differentiation, glioblastoma, IDH mutation, REST, KAISO, ZBTB33, DNA methylation, transcription factor, extracellular matrix, invasion

Introduction

REST (RE1-silencing transcription factor), previously known as NRSF – the neuron-restrictive silencer factor, participates in the control of neuronal differentiation, regulating the transition from stem to progenitor cells (Ballas et al., 2005). REST and its co-repressor complex participate in shaping neuronal plasticity in developing brains, as well as repressing neuronal gene expression in non-neuronal terminally differentiated cells (Ballas et al., 2005). REST is also one of the most prominent players in glioblastoma stem cells regulating their tumorigenic potential (Kamal et al., 2012). REST may recruit many epigenetic factors that in turn can repress or activate gene expression by imprinting active or repressive marks on histones and DNA (Ballas et al., 2005; Lee et al., 2005; Noh et al., 2012; Pilotto et al., 2015). REST can recruit MECP2 – methyl-CpG binding protein 2 and as a part of CoREST/MeCP2 repressor complex can bind to methylated sites distinct from canonical RE1 sites (Ballas et al., 2005; Noh et al., 2012). We have recently shown that DNA methylation within the predicted REST binding sites has a prognostic value in patients with higher grade gliomas (Dabrowski et al., 2018). Moreover, increased expression of genes putatively regulated by REST correlates with poor prognosis of glioma patients (Liang et al., 2016). REST appears as a transcription factor which expression correlates well with its activity and its activity can be well inferred from the expression of its targets (Liang et al., 2016).

Mutations in genes coding for IDH1 or IDH2 (isocitrate dehydrogenases) occur frequently in WHO grade II/III gliomas and secondary glioblastomas and result in global changes in DNA methylation. IDH mutant (IDH-MUT, most commonly R132H substitution) apart from α -ketoglutarate (α-KG), produces 2-hydroxyglutarate (2HG) (Dang et al., 2009) that can inhibit α-KG-dependent dioxygenases such as DNA and histone demethylases (Xu et al., 2011). As DNA and histone demethylation are inhibited, cells are blocked in the hypermethylated epigenetic state, which dysregulates expression of genes and blocks cell differentiation (Flavahan et al., 2016; Turcan et al., 2018). Whole genome epigenetic changes related to IDH1/2 mutations are often described as IDH-related phenotype (J. Dabrowski and Wojtas, 2019).

REST can bind both unmethylated and methylated DNA in various contexts (Kamal et al., 2012; Stadler et al., 2011; Zhang et al., 2017). Knockdown of REST in glioblastoma (GBM) xenografts significantly impairs tumor growth (Conti et al., 2012). The authors proposed that REST inhibits expression of neuronal lineage genes in glioma cells, leading to self-renewal and increasing tumorigenic potential of cells, while in the cells with REST knockdown, the inhibition of neuronal genes is abolished, leading to either cell differentiation or cell death (Conti et al., 2012). The role of REST in gliomas is far from conclusive. On one hand, the inhibition of REST in established human U87 and U251 glioma cells resulted in reduced cell proliferation and migration (Zhang et al., 2016). On the other hand, REST and p53-deficient mice develop glioblastomas that are similar to human proneural tumors with some characteristics of primitive neuroepithelial tumors (PNET) (Nechiporuk et al., 2016). Therefore, the role of REST varies depending on a cell origin and its developmental stage, suggesting it could be context dependent.

In the present study, we sought to determine at genome-wide perspective, whether inhibiting and activating functions of REST in glioma cells are modified by the IDH status and inferred changes in DNA methylation in gliomas.

Results

REST expression is positively correlated with glioma malignancy and IDH mutation

We analyzed *REST* expression in the Cancer Genome Atlas (TCGA) transcriptomic data encompassing normal brain (NB) tissues, LGG (Lower Grade Gliomas, WHO grades II and III) and GBM (glioblastoma, WHO grade IV) samples. The expression of *REST* was the lowest in normal brain tissue and the highest in the WHO grade IV gliomas (GIV), with *REST* expression increasing with grade malignancy from grade II (GII), through grade III (GIII) to grade GIV (Figure 1A). The differences in *REST* expression in NB, GII, GIII and GIV were significant (adjusted p-value < 0.001). Interestingly, within the LGGs, *REST* expression was significantly higher in *IDH1/2* mutated (IDH-MUT) gliomas than in wild type samples (IDH-WT) (Figure 1B; two-sample Wilcoxon test).

Next, we investigated whether *REST* expression had a prognostic value in glioma patients' survival. We confirmed that *REST* expression level is a strong negative prognostic factor for patient's survival in the joint cohort of LGG and GIV samples. Patients with low *REST* expression had a favorable prognosis (Figure 1C, top left). When analyzed separately, patients with IDH-WT GBMs and high *REST* expression had longer survival (Figure 1C top right), contrary to patients with IDH-MUT LGGs (Figure 1C, bottom left) and IDH-WT LGGs (Figure 1C, bottom right), where high *REST* expression was associated with shorter survival. However, the results of IDH-WT LGG must be taken with caution since a sample size was small due to a scarcity of those tumors.

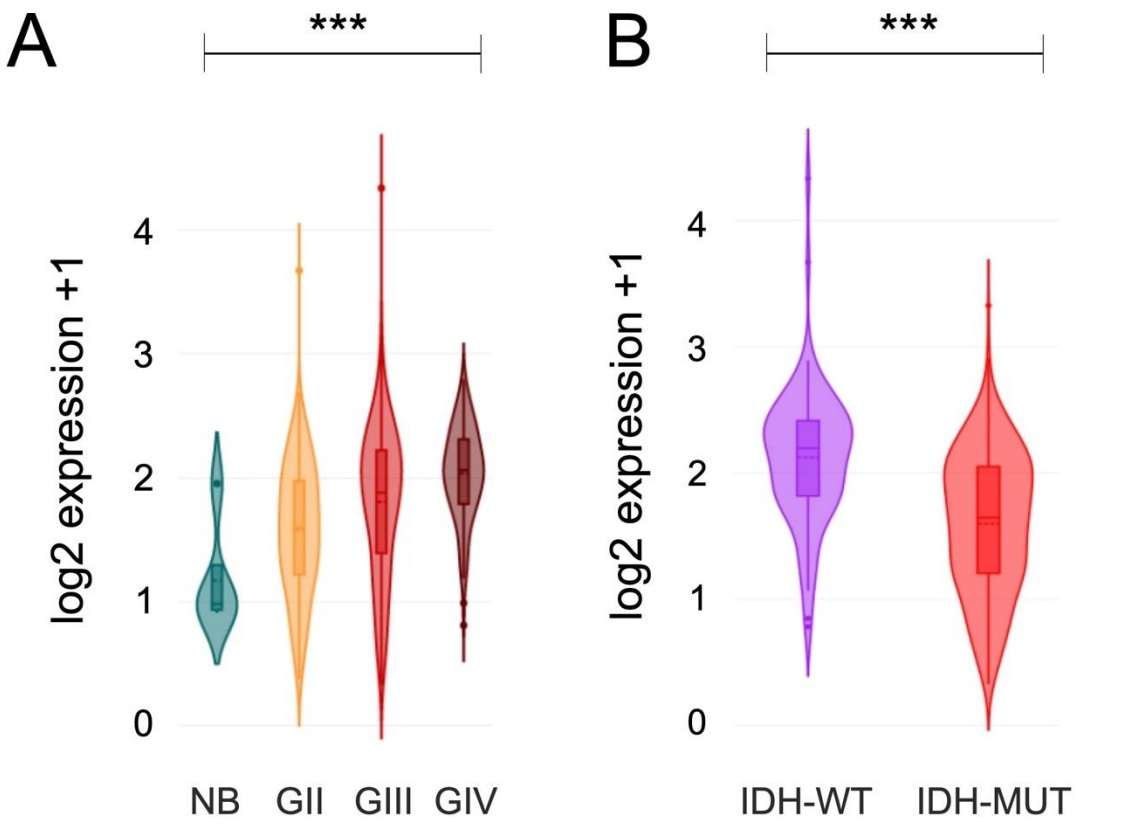

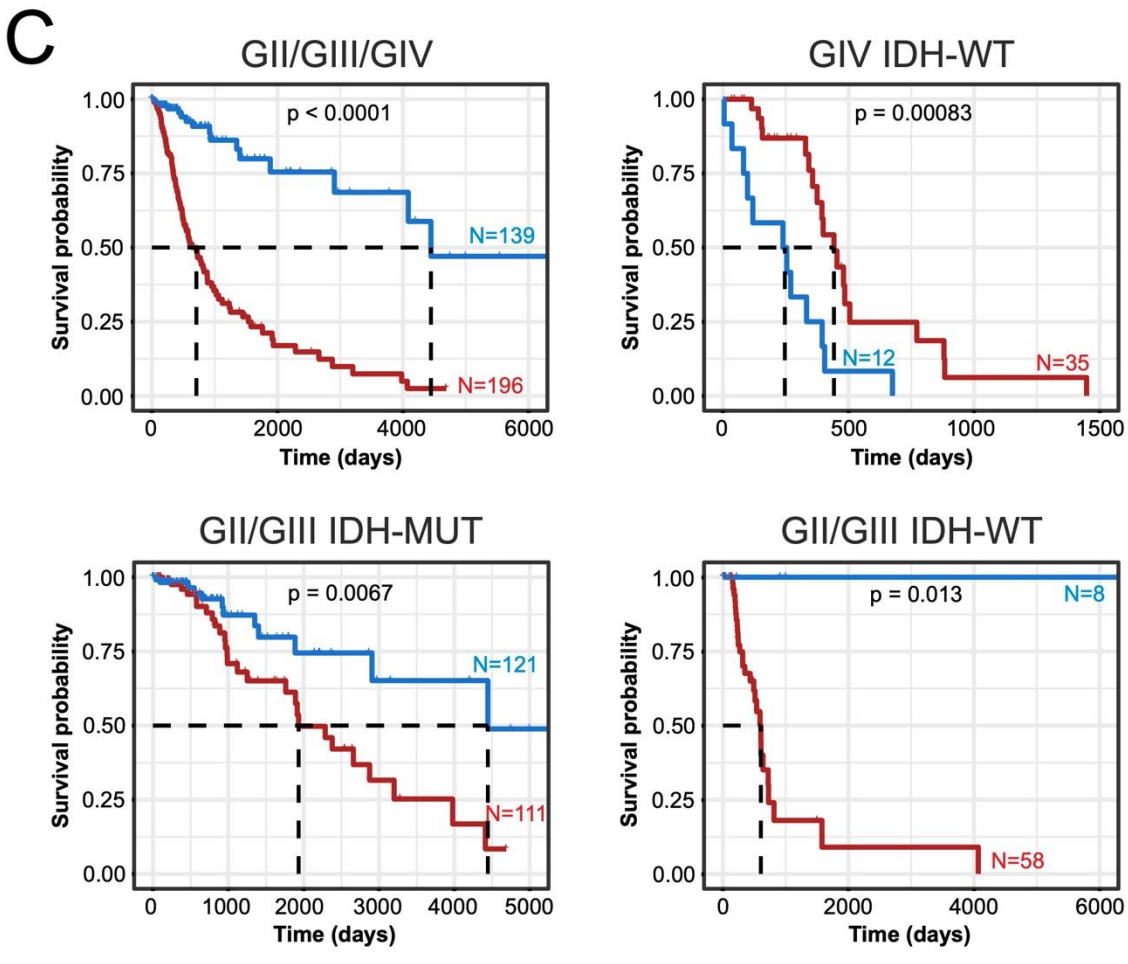

Figure 1. *REST* expression and survival analysis in the glioma TCGA dataset.
(A) Violin plots showing expression of *REST* in a TCGA dataset across different glioma grades and normal brain. Significance of difference in gene expression was calculated with the Welch's ANOVA test.
(B) Violin plot showing *REST* expression between *IDH1* wild type and *IDH1* mutants in GII/GIII gliomas (statistical significance calculated with the two-sample Wilcoxon test).
(C) Kaplan-Meier overall survival curves for the patients with WHO grade II, III, and IV glioma (top left); IDH-WT WHO GIV glioma (top right); IDH-MUT WHO GII/GIII glioma (bottom left); WHO grade II and III IDH wild-type (bottom right). The patients were divided into high or low *REST* expression groups. The patients alive at the time of the analysis were censored at the time of the last follow-up. Statistical significance was computed using the Log Rank Test.

Differentially expressed genes in human IDH1-WT and IDH1-MUT U87 cells and the TCGA dataset

We reasoned that before performing experiments on the U87 cell lines we will investigate their transcriptomes and compare them to tumor samples to validate this model. We took advantage of having isogenic U87 glioma cells with different *IDH1* status and analyzed transcriptomic profiles of U87 IDH-WT and U87 IDH-MUT glioma cells. We found significant differences in gene expression confirming transcriptomic deregulation (Figure S1A). The REACTOME pathway analysis of differentially expressed genes (DEGs) in IDH-WT and IDH-MUT cells revealed a vast number of genes associated with extracellular matrix (ECM) and its reorganization (Figure S1B). Interestingly, when DEGs identified in U87 cells were compared with the TCGA dataset a set of genes down-regulated in U87 IDH-MUT as compared to U87 IDH-WT was highly concordant with a set of genes down-regulated in IDH-MUT versus IDH-WT gliomas from TCGA (61% concordance, Figure 1A). Only TCGA LGG samples were included into this comparison because a number of IDH-MUT GIV samples was insufficient. Application of the bootstrapping method with 10,000 sampling ensured that such concordance is unlikely to be random as none of the bootstrapped results returned such a high concordance. The overlap of up-regulated genes between glioma cells and TCGA gliomas was smaller (38%), which was less than the median overlap (48%) returned by bootstrapping. Genes up-regulated in IDH-MUT U87 cells were enriched in REACTOME pathways that were dissimilar to those detected in LGGs (Figure S1C). The REACTOME pathways of down-regulated genes in U87 IDH-MUT vs IDH-WT were highly similar to those from IDH-MUT vs IDH-WT in LGGs (Figure S1D). Altogether, patterns of down-regulated genes in IDH-MUT U87 glioma cells resulting from the hypermethylator phenotype well reflect changes detected also in IDH-MUT LGGs, while in case of up-regulated the concordance is moderate.

REST knockdown in glioma cells affects numerous biological processes

To find REST dependent genes in glioma cells with different IDH1 status we performed siRNA mediated knockdown of REST (siREST) in IDH-WT and IDH-MUT U87 cells. A significant reduction in REST mRNA (Figure 2B) and protein (Figure 2C) levels was observed after 72 hours of REST silencing in both U87 cell lines. REST mRNA levels were reduced by 77% in IDH-MUT, and by 82% in IDH-WT (Figure 2B), while REST protein levels were reduced by 89% in IDH-MUT and by 90% in IDH-WT as compared to control siRNA (siCTRL) transfected cells (Figure 2C).

We compared transcriptomic profiles between siREST and siCTRL cells and identified 1,356 DEGs in IDH-WT cells and 629 in IDH-MUT (Figure 2D). Out of 1,356 DEGs, 507 were common for IDH-WT and IDH-MUT cells. The majority of the common DEGs were up-regulated (n=287) after REST knockdown, whereas 220 DEGs were down-regulated, including *REST,* which had the highest log2 FC between siREST and siCTRL in both IDH-WT and IDH-MUT models (Figure 2C, D). The Gene Ontology Biological Processes (GO BP) functional analysis was performed independently for the siREST up- and down-regulated DEGs. The down-regulated DEGs were enriched in cell division-related pathways (Figure 2E, upper panel), whereas the up-regulated genes were enriched in neuronal-specific pathways, as well as pathways associated to endothelial cell proliferation and extracellular matrix organization (Figure 2E, bottom panel). However, analysis of IDH-WT vs IDH-MUT in both U87 cell lines and tumors revealed that ECM-related pathways may be differentially regulated, pointing to REST as a potential modulator of this pathways depending on IDH status (Fig S1).

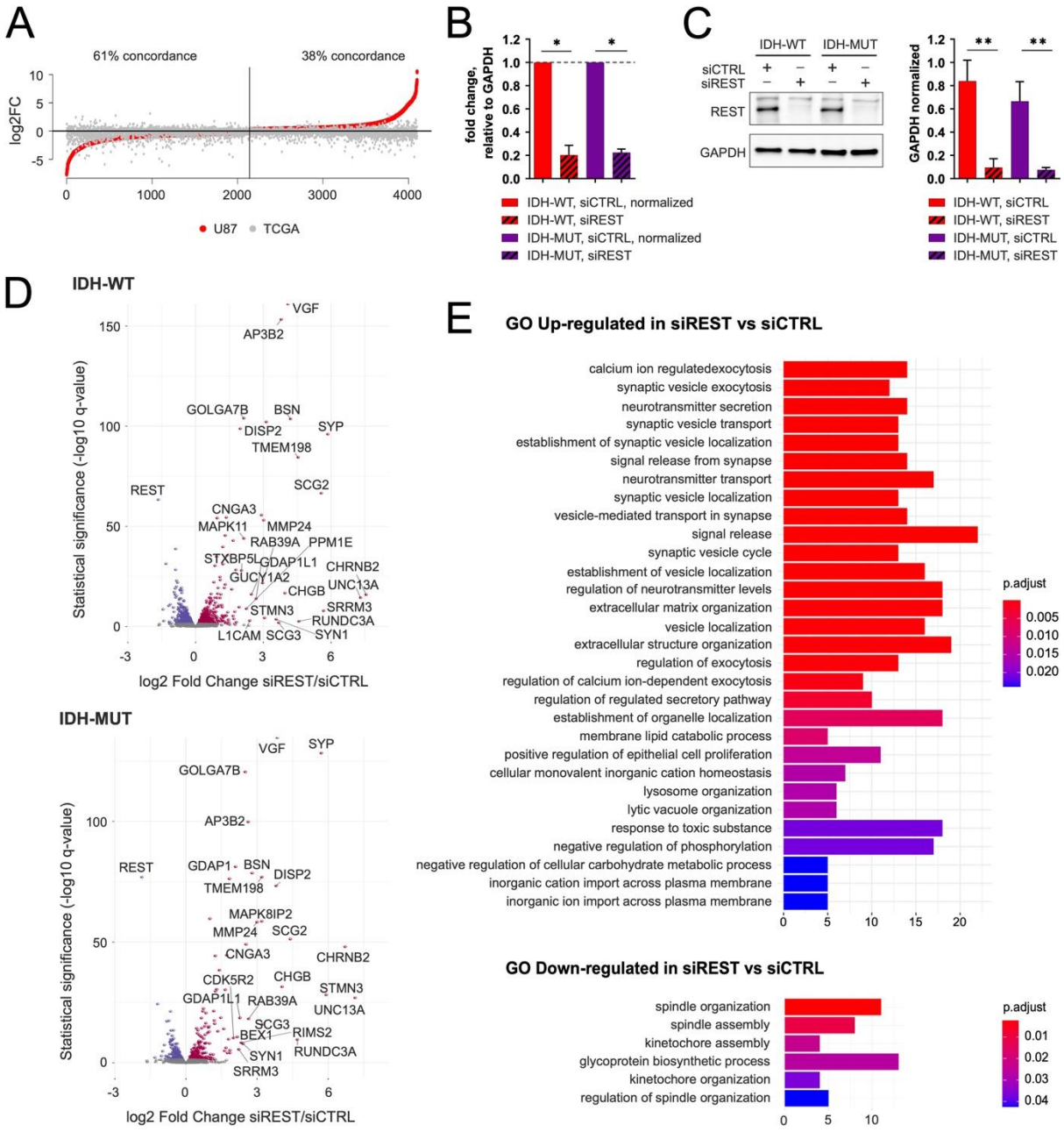

Figure 2. Effects of REST knockdown on gene expression in IDH-WT and IDH-MUT U87 cells.
(A) Sorted values of log2 fold change (log2 FC) for the genes coming from the IDH-MUT vs IDH-WT comparison in U87 cell lines were presented as red dots. Values for the same genes coming from IDH-MUT vs IDH-WT comparison in TCGA GII/GIII gliomas were overlaid as gray dots. Percent of log2 FC direction concordance between IDH-MUT vs IDH-WT in U87 cell lines and glioma tumors was calculated. Number of differentially expressed genes is indicated. Black vertical line separates genes expressed higher in IDH-MUT U87 compared to IDH-WT U87 from the genes expressed higher in IDH-WT U87 compared to IDH-MUT U87.
(B) Relative expression of REST in IDH-WT and IDH-MUT U87 cells at 72 hours of REST silencing with siRNA. mRNA levels in transfected cells were determined with quantitative PCR and normalized to GAPDH expression in the same sample. Data are represented as mean ± SEM, n=4 independent experiments, * $p<0.05$, two-tailed Mann-Whitney test (WT: p=0.0286; MUT: p=0.0286).
(C) Levels of REST protein in IDH-WT and IDH-MUT U87 cells at 72 hours after transfection with control or REST specific siRNAs determined with Western blotting. Immunoblots were analyzed densitometrically. Data are represented as mean ± SEM, n=4. **$p<0.01$ (WT: p=0.0018, MUT: p=0.0052; two-tailed ratio-paired t-test). No difference was observed in the level of REST protein between silencing controls (siCTRL) in IDH-MUT and IDH-WT (p=0.226).
(D) Volcano plots of the differentially expressed genes between siCTRL and siREST in IDH-WT (upper plot) or IDH-MUT (bottom plot) U87 glioma cells. The axes show log2 FC (x-axis) and -log10 from adjusted q-value (y-axis).
(E) Gene Ontology (GO) Biological Processes (BP) analysis was performed on DEGs common in IDH-WT and IDH-MUT. The results are presented as bar plots for pathways down-regulated (upper panel) and up-regulated (bottom panel) in REST depleted cells.

Regulation of gene expression by REST depends on *IDH1* mutation status

To evaluate an impact of REST on gene regulation in the context of *IDH1* mutation, we performed three pairwise comparisons of transcriptomic profiles between IDH-WT and IDH-MUT. Differential analysis between IDH-WT vs IDH-MUT was performed for the untreated, siCTRL-transfected and siREST-transfected U87 IDH-WT and IDH-MUT cell lines. DEGs identified in these comparisons were intersected (Figure 3A) to validate utility of our cell line model and pinpoint silencing-specific effects. We discovered 2,943 IDH-DEGs common for the three comparisons (Figure 3A), showing a strong influence of the IDH-related phenotype on gene expression. To investigate the effect of REST knockdown on IDH-phenotype dependent genes, we focused on genes significantly altered in REST depleted cells (n=6,626) (Figure 3A, delimited in a grey circle) and compared DEGs fold changes in control and REST depleted cells. IDH-MUT/WT DEGs with similar fold changes were considered REST independent (Figure 3B). Increased DEGs (iDEGs) were defined as DEGs with a higher fold change in siREST-transfected cells (log2 FC>0.25, Figure 3C), while those with lower fold change in siREST-transfected cells (log2 FC<-0.25) were considered decreased DEGs (dDEGs). We defined DEGs as iDEGs when they had log2 FC difference between siREST and siCTRL above 0.25 and dDEGs as those that had log2 FC lower than -0.25 (Figure 3C).

The GO BP pathway analysis performed on these selected genes demonstrated that iDEGs showed the enrichment in genes involved in extracellular matrix (ECM) organization and negative regulation of neuron differentiation (Figure 3D). Within these pathways, the

highest log2 FC increase was observed in several integrin (*ITGAD*) and metalloproteinases (*MMP10*) encoding genes. Moreover, the enrichment in genes related to reproductive, developmental, glial differentiation pathways and positive regulation of leukocyte activation was found (Figure 3E). Increased expression of genes related with ECM in IDH-MUT REST depleted cells and decrease in expression of these genes in REST depleted IDH-WT cells, contrasted with decreased expression of glial differentiation related genes in IDH-MUT REST depleted or increased expression of these genes in REST depleted IDH-WT (Figure 3F).

These findings point to a potential role of REST in a switch between ECM organization and cell differentiation in cells with the IDH-related phenotype.

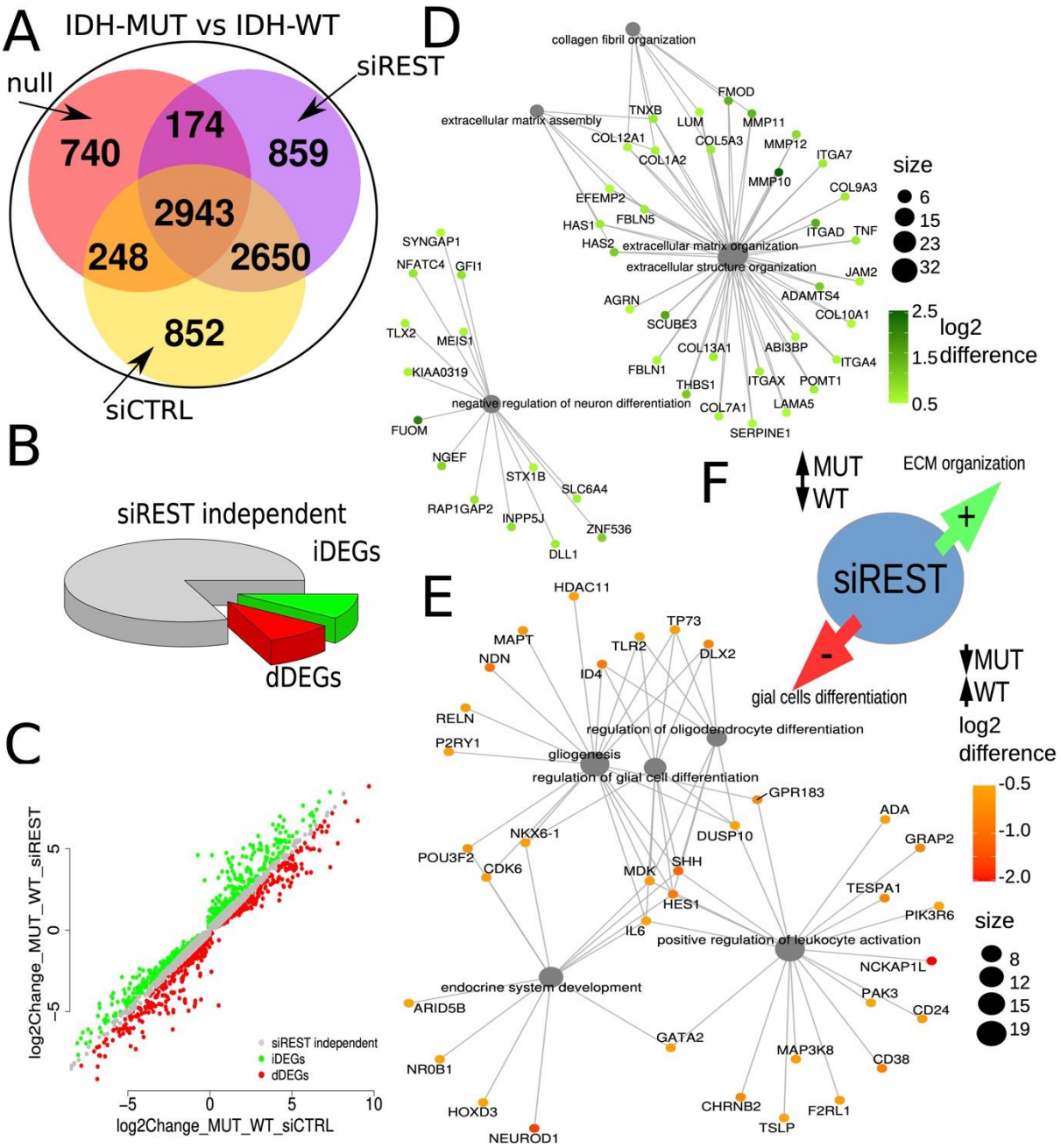

Figure 3. REST knockdown differentially affects expression of genes involved in extracellular matrix (ECM) organization and glial cell differentiation in IDH-WT and IDH-MUT glioma cells.

(A) Venn diagram showing the overlap of the differentially expressed genes between IDH-WT vs IDH-MUT in untreated, siREST or siCTRL-transfected U87 glioma cells. Grey circle marks DEGs in the siREST IDH-WT and IDH-MUT cells.
(B) Subsets of IDH-DEGs altered (red, green) or unchanged in REST depleted cells (grey).
(C) Comparison of the fold change difference in gene expression in the cells with wild type or mutated IDH, following siREST/siCTRL transfection. In siREST-transfected cells, a group of DEGs showed a shift in log2 fold change (log2 FC) between IDH-MUT and IDH-WT in siREST compared to siCTRL-transfected cells. Shift of IDH-MUT vs IDH-WT log2 FC in siREST transfected cells when compared to siCTRL transfected cells was either up (green, increased DEGs, iDEGs) or down (red, decreased DEGs, dDEGs). Difference in log2 FC was assumed significant when log2 FC shift between IDH-MUT and IDH-WT comparisons in siREST and siCTRL was > 0.25 and adjusted p-value < 0.05.
(D) Gene Ontology Biological Processes (GO BP) pathways analysis of the iDEGs, showing genes associated with ECM matrix organization and negative neuronal differentiation.
(E) Gene Ontology Biological Processes (GO BP) pathways analysis of the dDEGs, showing genes associated with glial differentiation and immune/endocrine pathways.
(F) Graphical summary showing the opposite effect of REST knockdown in IDH-WT and IDH-MUT on the expression of genes related to ECM organization and cell differentiation.

The effect of REST knockdown on glioma cell invasiveness and expression of genes associated with extracellular matrix depends on the *IDH* mutation - related phenotype

We tested whether the enrichment in Gene Ontology biological pathways related to ECM organization and cell differentiation observed in REST depleted glioma cells coexisted with changes in the invasiveness and viability of the cells. Viability of both IDH-WT and IDH-MUT glioma cells was not significantly affected by REST knockdown at 12-, 24-, 48- or 72 hours post-transfection as measured with the PrestoBlue assay (Figure 4A). The invasion of REST depleted IDH-WT cells quantified with Matrigel assay increased by 75% compared to control cells (Figure 4B). The opposite trend, observed in IDH-MUT, was not statistically significant. Invasiveness of the siCTRL cells was strongly influenced by their IDH mutation status (Figure 4B).
DEGs whose fold change between IDH-MUT and IDH-WT was increased by REST (iDEGs, Figure 3D) included a group of genes implicated in the ECM organization pathway (Figure 4C). To validate if these genes depend on REST in the tumor transcriptome dataset, their expression was correlated with *REST* expression using TCGA glioma dataset (GII-GIV). Majority of them significantly correlated with *REST* either in GIV (Figure S2, left), LGG IDH-MUT (Figure S2, middle) or in LGG IDH-WT (Figure S3, right), supporting the notion that REST is required to regulate ECM-related gene expression but its targets may differ depending on the IDH-MUT status. Finally, using tumor methylome data of IDH-WT and IDH-MUT (GII/GIII) gliomas, hereafter “Glioma Atlas” (Stępniak et al., 2021), we found that 16 out of the 32 identified ECM related genes had differential DNA methylation in gene promoters (Figure 4D) and 11 within gene bodies (Figure 4E).

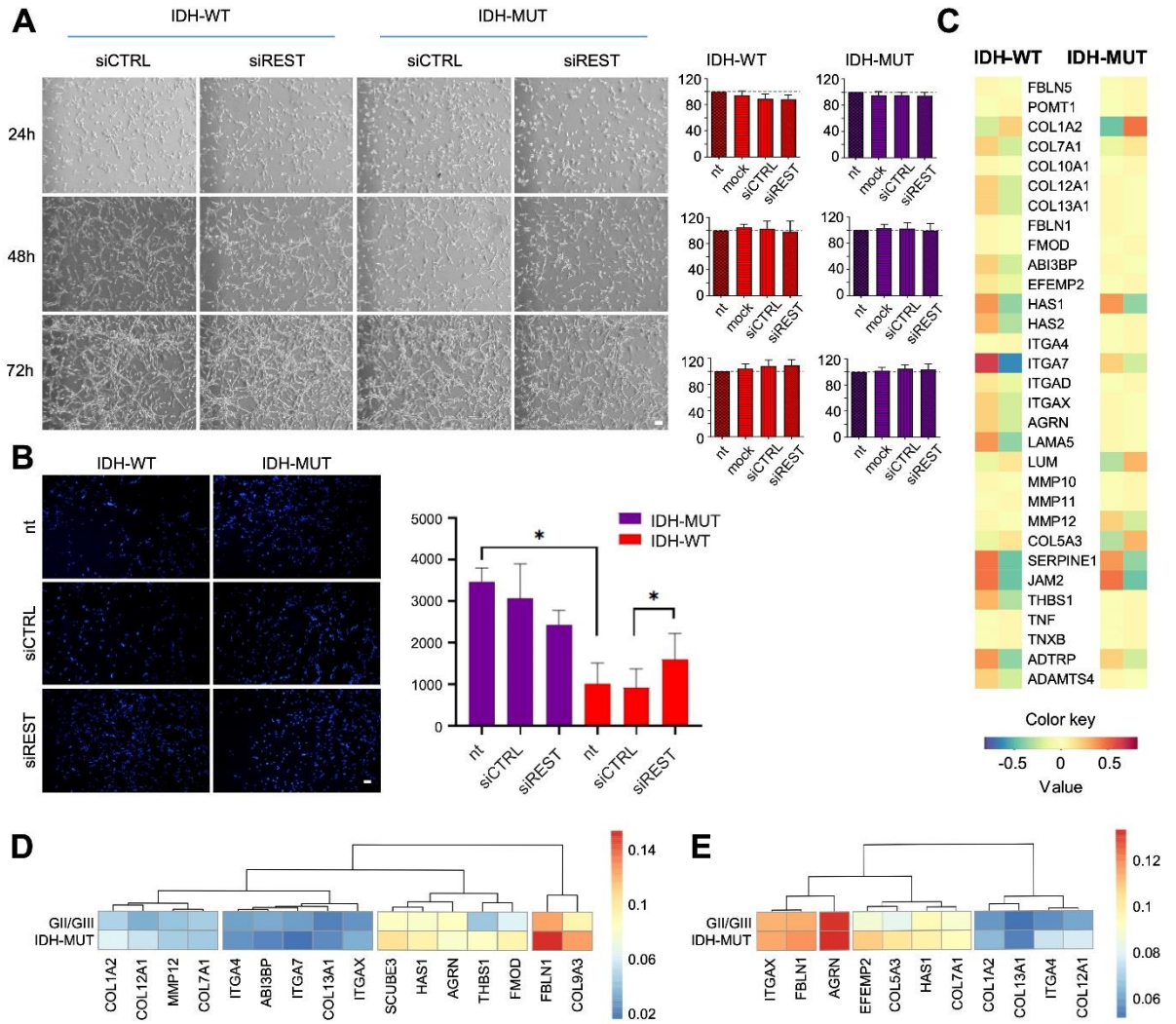

Figure 4. REST knockdown affects glioma cell invasiveness and expression of genes implicated in cell migration/invasion.

(A) Bright field microscopy images of IDH-WT and IDH-MUT U87 cells 24-, 48- and 72 hours after siRNA transfection; scale bar = 200 µm. Cell viability after 24-, 48- or 72 hours of REST silencing measured with PrestoBlue assay. Data are represented as mean ± SEM, n=3, Wilcoxon matched-pairs signed rank test, two-tailed ($p>0.05$). Dotted line at 100% denotes a viability of mock-transfected cells.

(B) Invasiveness of IDH-WT and IDH-MUT U87 cells measured with Matrigel invasion assay. The cells were either not treated (nt) or transfected with siCTRL or siREST. The fluorescence microscopy images (scale bar = 200 µm) show representative fields of Matrigel inserts and the bar plot shows quantification of the migrating cells. Data are presented as mean ± SEM, n=6, *$p<0.05$, Wilcoxon matched-pairs signed rank test. IDH-WT: siCTRL: 908.8 ± SEM=460; siREST: 1597± SEM=622.3. Not treated cells: IDH-MUT: 3472 ± SEM=324.7; IDH-WT: 1019 ± SEM=490.6; p=0.0313.

(C) Extracellular matrix organization GO BP-related IDH-DEGs modulated by siREST (selected from functional analysis from Figure 3C) presented as a heatmap for IDH-WT (left panel) and IDH-MUT (right panel) siREST (right column in each panel) vs siCTRL (right column in each panel) U87 glioma cell lines.

(D-E) Hierarchical clustering based on mean DNA methylation level **(D)** within promoters (TSS -2000/+500 bps) and **(E)** gene bodies of ECM genes whose DNA methylation was significantly different between IDH-MUT and IDH-WT (GII/GIII) tumor samples deposited in Glioma Atlas.

Characterization of REST ChIP-seq peaks in IDH-WT and IDH-MUT U87 cells

Chromatin immunoprecipitation followed by sequencing (ChIP-seq) was employed to identify REST binding sites in U87 glioma cells. The analysis revealed almost four thousand REST ChIP-seq peaks out of which 2,647 were common in IDH-WT and IDH-MUT cells, while 114 were specific to IDH-MUT and 1,077 to IDH-WT cells. REST-ChIP-seq peaks were annotated to genes (hereafter referred to as REST targets). Consistently, the majority of REST targets were shared between IDH-WT and IDH-MUT cells (n=1,674), but 85 genes were specific to IDH-MUT and 860 IDH-WT cells (Figure 5A). Most of the IDH-MUT specific peaks were located in the intergenic or intronic regions, while the IDH-WT were located mainly in gene promoter regions (Figure 5B). Both, the lower number of binding sites identified in IDH-MUT (Figure 5A) and more distal IDH-MUT specific binding sites localization from transcription start site (Figure 5B) indicates that role of REST in IDH-MUT is different than in IDH-WT.

The REACTOME pathway analysis of genes annotated to REST peaks indicated the gene enrichment in ten pathways common to IDH-WT/MUT and eleven pathways specific to either IDH-WT or IDH-MUT REST targets (Figure S4A). Ten of these pathways were specific to IDH-WT, and they were related to transcription, translation, nonsense mediated decay, voltage gated potassium channels, infectious disease, and heat shock factor 1 activation. The only pathway significantly enriched in targets specific to IDH-MUT was: “Interaction between L1 and ankyrins” (Figure S4A).

Next, we examined sequences of REST ChIP-seq peaks assigned to genes specific to IDH-WT (n=860), IDH-MUT (n=85), or common to both cell types (n=1,674) (Figure 5A) to find transcription factors (TFs) binding sites within these regions and identify TFs whose binding might depend on the IDH-related phenotype. Using the EnrichR tool and the ENCODE ChIP-seq dataset, we identified TFs overlapping within REST-ChIP-seq peaks (Figure S4C). In particular, we found that ENCODE ChIP-seq peaks of KAISO known also as ZBTB33 (Zinc Finger and BTB Domain Containing 33) had the strongest enrichment within the REST-ChIP-seq peaks specific for IDH-WT cells (Figure S4C middle panel). In IDH-MUT specific REST-ChIP-seq peaks, only REST motifs were identified (Figure S4C, middle panel), while in the REST-ChIP-seq peaks common for the IDH-WT and IDH-MUT, REST motifs appeared at the top positions of the enrichment ranking, but at the lower positions, KAISO motifs were present as well (Figure S4C, top panel).

KAISO transcription factor has been reported in several different human cancers functioning as a tumor suppressor or oncogene (Blattler et al., 2013). KAISO function seems to be highly context-dependent (Pierre et al., 2019a). It binds to methylated CpGs in two motifs within a consensus sequence 5’-CGCG-3’ (Figure 5C and D: KAISO.0.A and KAISO.1.A) and to unmethylated C in the motifs with another consensus sequence 5’-CTGCNA-3’ (Figure 5C and D: KAISO.2.A) (Blattler et al., 2013).

To identify specific TF motifs, present within the REST ChIP-seq peaks specific for IDH-WT or IDH-MUT, or common for both IDH-WT and IDH-MUT, we investigated the peak sequences using all available position weighted matrices (PWMs) deposited in the **HO**mo sapiens **CO**mprehensive **MO**del **CO**llection (HOCOMOCO) database (version 11) and additional 14 REST PWMs from the ENCODE dataset. Using the R PWMEnrich package and

the FIMO tool (Grant et al., 2011), we identified 14 motifs in IDH-MUT specific REST-ChIP-seq peaks, 70 in IDH-WT-specific and 120 in the common peaks (Figure S4B). Ten motifs were shared among the common, IDH-WT and IDH-MUT REST ChIP-seq peaks (Figure S4B). Focusing on KAISO motifs, we discovered that all the three HOCOMOCO motif variants (0.A, 1.A and 2.A) were present within the common and the IDH-WT-specific REST ChIP-seq peaks, but not in the IDH-MUT-specific peaks (Figure S4D).

We hypothesized that changes in DNA methylation resulting from an IDH mutation may affect binding of REST to its respective sites. Therefore, we examined DNA methylation levels within all the REST-ChIP-seq peaks detected in the U87 cells. We analyzed methylome data from the recently published Atlas of Brain Regulatory Regions (Stępniak et al., 2021) using the DiffMeth tool. DNA methylation level was determined in GII/GIII IDH-MUT, GII/GIII IDH-WT and GIV IDH-WT glioma samples. Pairwise comparisons of DNA methylation between different glioma samples were performed separately for the sequences in U87 REST ChIP-seq peak assigned as common, IDH-WT or IDH-MUT specific (Figure S5A-C). A similar percentage of common, IDH-WT and IDH-MUT specific peaks was differentially methylated: 8%, 6.9%, 5.5% respectively. The largest number of differentially methylated peaks was detected between a pair of GII/GIII IDH-MUT vs GIV IDH-WT samples (Figure S5A-C, middle column). Next, to identify the effect of IDH-related phenotype, we focused on peaks differentially methylated between IDH-WT and IDH-MUT GII/GIII/GIV samples (Figure S5A-C, left column). In majority of cases IDH-MUT samples had higher DNA methylation (Figure S5D-F), showing that rather IDH mutation status then peak origin impacts more on differential DNA methylation pattern of REST ChIP-seq peaks in glioma tumors.

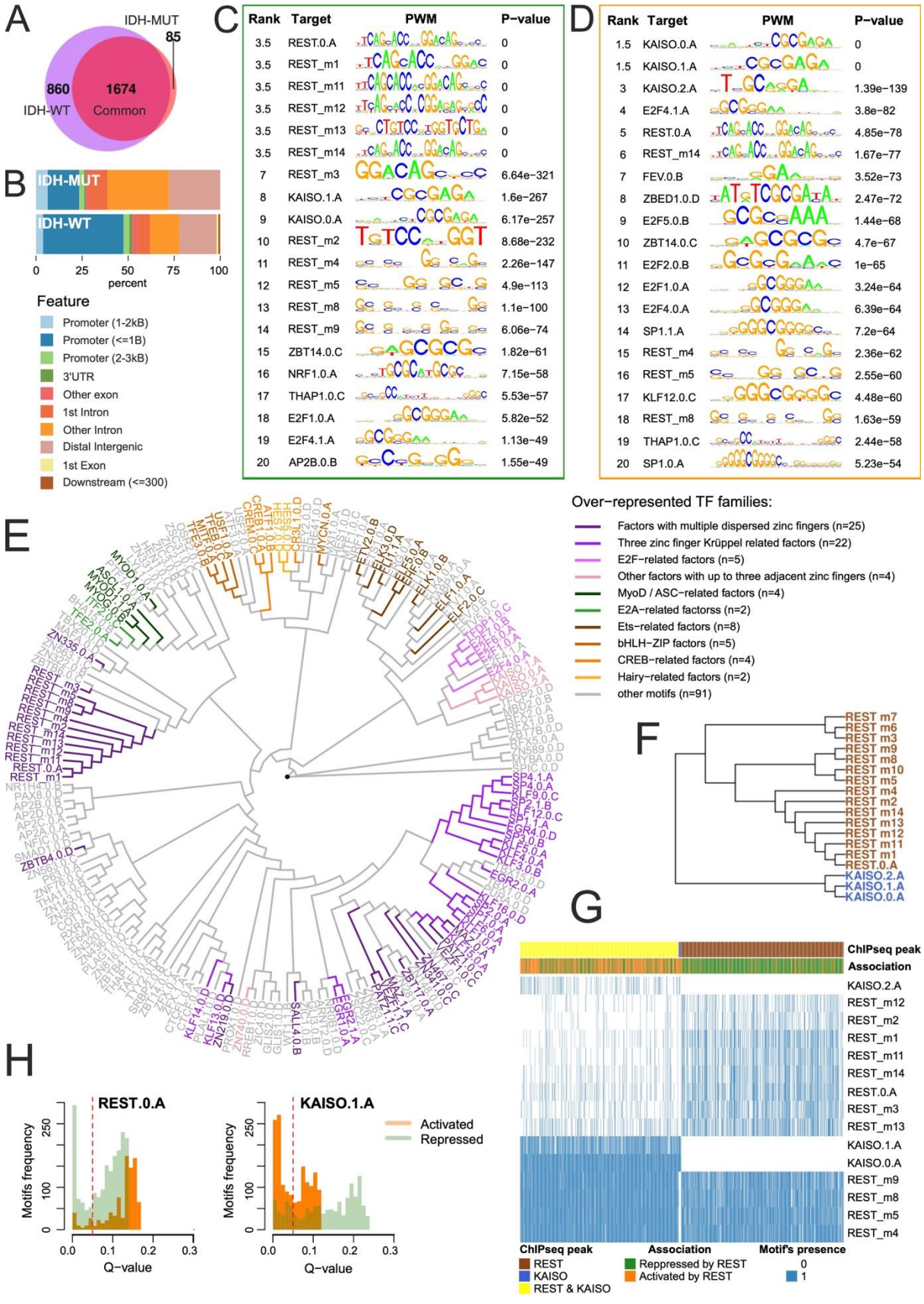

Figure 5. Characterization of REST ChIP-seq peaks and their target genes.

(A) Intersection of genes assigned to REST ChIP-seq peaks in IDH-WT and IDH-MUT U87 cells. Peaks were assigned to genes following the R ChIPseeker library assignment to the promoter region.
(B) Annotation of identified REST ChIP-seq peaks to genomic regions.
(C-D) Ranking of the TOP 20 TF motifs identified in the sequences of the REST ChIP-seq peaks assigned to genes repressed by REST **(C)** or activated by REST **(D)**. Briefly, *REST* expression was correlated with the genes to which REST-ChIP-seq peaks were assigned (called REST targets) using TCGA dataset (data from the Figure 5A). Based on the correlation results between *REST* gene expression and REST targets, the genes were divided into repressed or activated by REST. If correlation was statistically significant (adjusted p value <0.05) and correlation coefficient was positive, a gene was assigned as activated by REST, while coefficient was negative, a gene was assigned as repressed by REST.
(E) Hierarchical tree of TF motifs for enriched TF families based on PWMs. Shades of green represent motifs from TF protein families overrepresented in REST ChIP-seq peaks unique for repressed REST targets; orange - activated; magenta - motifs overrepresented in the group of motifs present in both repressed and activated REST targets.
(F) REST and KAISO (ZBTB33) motifs clustering based on PWMs.
(G) Hierarchical clustering of REST peaks according to the identified KAISO and REST motifs. Color-coded bars show the association of a REST peak and its target gene, impact on gene expression (repressed or activated by REST) and the presence of REST or KAISO motifs.
(H) Q-value and frequency relations for selected KAISO (ZBTB33) and REST motifs within REST ChIP-seq peaks assigned to genes activated or repressed by REST. To highlight the pattern, bar plots show the full distribution of q-values with a red dashed line indicating significance cut-off point.

Variability of TF motifs within the REST ChIP-seq peaks

Using TCGA LGG and GBM datasets, we correlated expression of *REST* and its targets. For the purposes of this study, we considered REST targets whose expression was negatively correlated with *REST* expression to be REST-repressed, whereas positively correlated as REST-activated. Most REST-repressed genes were enriched in the GO biological pathways related to neuronal functions, confirming its canonical role as a repressor of neuronal genes in non-neuronal cells (Figure S6A, left panel). On the other hand, pathways related to the REST-activated targets were more diverse (Figure S6A, right panel).

To determine the exact locations of the detected TF motifs in REST-activated and REST-repressed genes, we used the FIMO tool and identified 145 motifs for 119 TFs within the REST peaks assigned to REST-repressed genes and 140 motifs for 115 TFs within the peaks assigned to REST-activated genes (q-value ≤ 0.05). Hierarchical clustering tree of these TF motif PWMs revealed grouping of REST-repressed and REST-activated gene specific motifs (Figure S6B). The same tree, exhibiting TF motifs sequence similarities, was used to visualize protein families of TFs detected within REST peaks paired with REST-activated or repressed genes (Figure 5E). Among the motifs enriched in REST-ChIP-seq peaks of REST-repressed genes, were targets for ASCL1, MyoD and E2A-related factors that are engaged in cell differentiation and proliferation, including neuronal (ASCL1) and oligodendrocyte (E2A) differentiation (Sussman et al., 2002), mesenchymal cell proliferation (MyoD) and growth inhibition (Loveys et al., 1996). In cancer, these TFs act as activators (ASCL1) or inhibitors of the cell cycle progression (E2A) (Andrysik et al., 2013; Zhao et al., 2019). Motifs overrepresented in REST-activated genes were targets for CREB, Ets family proteins, bHLH-

ZIP, and Hairy-related factors. Among others, CREB regulates transcription of the genes coding for a proto-oncogene c-Fos (Chan et al., 1999) and neuropeptide VGF (Rodríguez-Seoane et al., 2015). The latter was one of the stronger up-regulated genes upon REST knockdown (Figure 2D). Ets family proteins are activated by Ras-MAP kinase signaling pathway and have been implicated in tissue differentiation and cancer progression (Oikawa and Yamada, 2003). Hairy-related proteins typically function as DNA-binding transcriptional repressors that have been shown to inhibit Notch activated *a-actin* (Tang et al., 2008) and control differentiation (Davis and Turner, 2001). Overrepresentation of the motifs for these TFs in the vicinity of REST binding sites in REST-repressed genes shows a potential contribution of their pathways to the diverse REST effects and its impact on tumorigenesis and patient survival.

To identify the most prevalent TF motifs within the REST peaks associated with REST-activated or REST-repressed genes, we performed TF motif scans using PWMs. The top of the ranking of the highest scoring motifs for the REST-repressed genes contained mainly REST motifs, as expected (Figure 5C). However, in the ranking of TF motifs in REST-activated genes, the first three positions were occupied by KAISO (Figure 5D). TF binding motif sequence logos generated for both KAISO and REST PWMs (Figure S6F, G) and hierarchical clustering of all discovered PWM sequences (Figure 5E) as well as REST and KAISO PWMs alone (Figure 5F) showed dissimilarity between these motifs, hence their co-occurrence within the REST ChIP-seq peaks was not due to the PWMs similarity. However, based on the distribution of the statistical significance of the occurrence of TF motifs, we may assume that KAISO motifs are more frequent in the promoters of REST-activated than REST-repressed genes, whereas REST motifs display a somewhat reverse pattern (Figure 5H). The results of CentriMo analysis showing the probability of REST or KAISO motif presence in the gene promoters corroborate this observation, as we found more frequent occurrence of KAISO motifs in genes activated by REST (Figure S6C) than in the genes repressed by REST (Figure S6D).

To determine a degree of REST ChIP-seq peaks similarity according to the detected REST and KAISO motifs, each peak was represented by a binary vector where a given REST or KAISO motif was present (value=1) or absent (value=0), and a hierarchical clustering on these vectors was performed (Figure 5G). In general, two clusters of peaks were discovered: 1) represented mostly by REST and KAISO motifs and associated with gene activation or 2) represented only by REST motifs and mostly associated with gene repression (Figure 5G). Among the reported REST peaks (n=1,523), 63% were related to repressed targets and 37% to activated targets. In the majority of peaks related to REST-repressed genes (69.5%), only REST motifs were found. In contrast, in the majority of peaks related to activated genes (81%) both REST and KAISO motifs were present. Our results imply, that KAISO motif occurrence or binding may be an important factor in REST-guided gene activation, but not in gene repression.

Distinct DNA methylation within REST and KAISO motifs in activated and repressed REST targets

DNA methylation contributes to activation or repression of transcription. DNA methylation can influence TFs binding and activity when occurring in the vicinity of their binding sites. While in the previous analysis (Figure S5) we verified DNA methylation of the whole 200 bp sequences of REST ChIP-seq peaks, here we focused on DNA methylation levels of REST

and KAISO motifs detected within the REST-ChIP-seq peaks assigned to REST-repressed or activated targets to verify whether DNA methylation may play a modulatory role in REST-guided gene regulation. We studied methylated cytosines in the CpG context with a minimal coverage of 10 reads in the GII/GIII/GIV IDH-MUT, GII/GIII IDH-WT and GIV IDH-WT glioma methylomes deposited in Glioma Atlas (Stępniak et al., 2021). These methylomes, covering millions of sites at 1 bp resolution, were intersected with coordinates of KAISO and REST motifs derived from U87 REST ChIP-seq. In result, we obtained 23,614 unique cytosines within TF motif sequences. The majority of cytosines occurred within either REST or KAISO motifs, but 2,588 were located within overlapping sites of REST and KAISO motifs. When a cytosine was located in multiple motifs of a single TF (due to motifs overlapping), its beta value (β) was only counted once. When a cytosine was located in overlapping motifs of different TFs (REST or KAISO), its beta value was counted separately for each TF motif. For each cytosine position, a mean methylation (β-value) across samples was computed and discretized into low [0-0.2], medium (0.2-0.6] or high (0.6-1]. Low β-values correspond to DNA hypomethylation, whereas high β-values indicate DNA hypermethylation. REST motifs in the REST ChIP-seq peaks lacking KAISO motifs and assigned to the repressed targets, were significantly enriched ($p<2.2x10^{-16}$) in medium- and hypermethylated cytosines (Figure 6A, Table S1). In these REST motifs, the percentage of hypermethylated cytosines was around three times higher than within REST-ChIP-seq peaks assigned to the activated REST targets (Figure 6A-B, Table S1).

Since a vast majority of cytosines were hypomethylated (Figure 6A-B), methylation variance across GII/GIII/GIV IDH-MUT, GII/GIII IDH-WT and GIV IDH-WT gliomas was computed for each cytosine within REST and KAISO motifs. The obtained variance ranged from 0 to 0.05 among sites, with an average β-value of 0.0067. To explore the methylation pattern within REST motifs, we selected cytosines with a higher variance than the average. We found that DNA methylation of REST motifs located within REST ChIP-seq peaks lacking KAISO motifs was significantly higher in peaks assigned to REST-repressed targets than in peaks assigned to REST activated targets across all glioma groups (Figure 6C). DNA methylation within REST motifs of REST ChIP-seq peaks containing both KAISO and REST motifs showed significantly higher DNA methylation in peaks assigned to repressed REST targets only in GIV gliomas (Figure 6D). In GII/GIII samples the methylation pattern was the opposite and in IDH-MUT no significant differences were detected (Figure 6D).

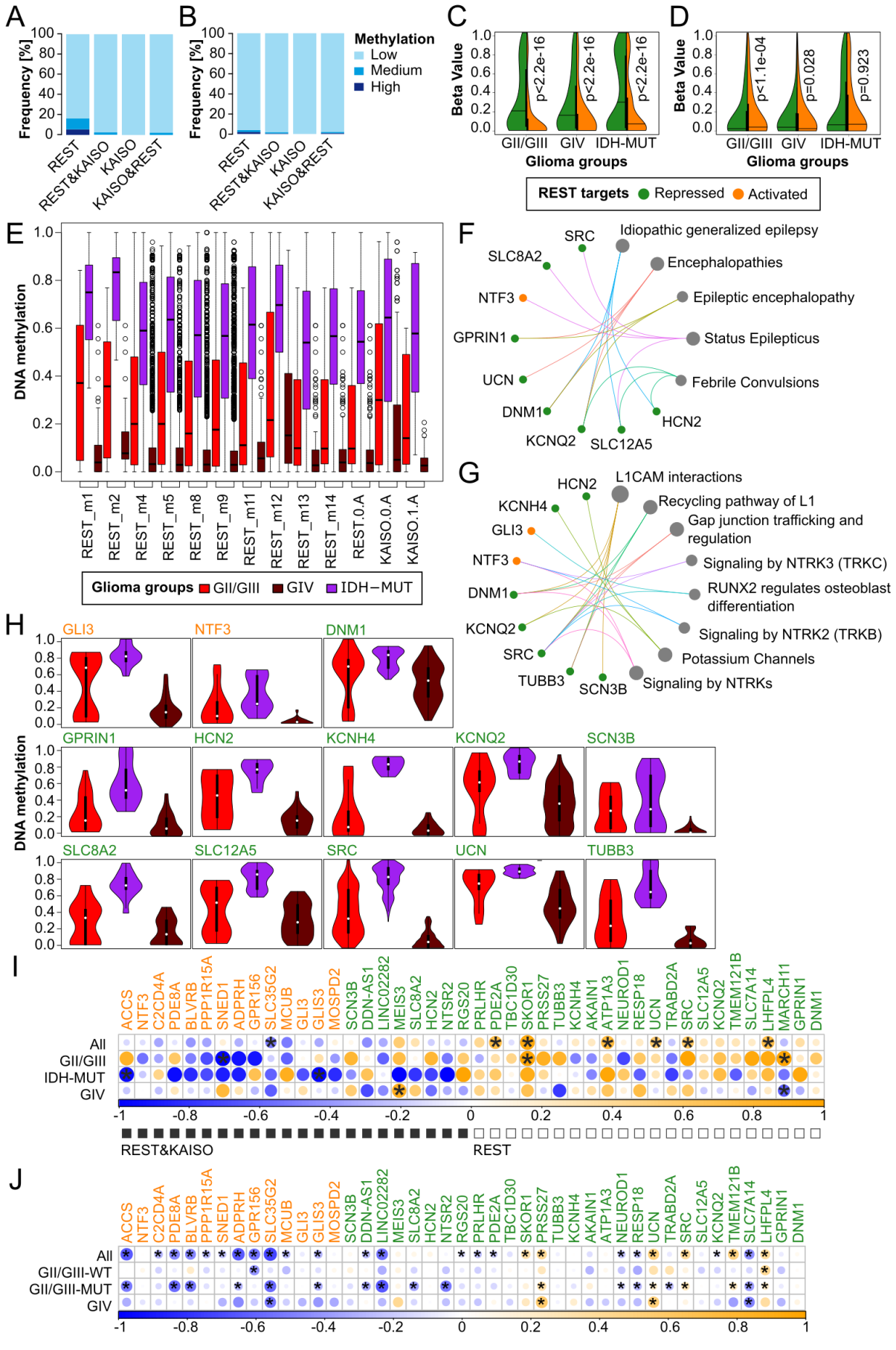

Figure 6. Distribution of DNA methylation at the selected REST ChIP-seq peaks and its influence on REST targets.

(A) DNA methylation of REST or KAISO motifs within REST ChIP-seq peaks assigned to REST-repressed targets. Description represents: REST – methylation of REST motifs of peaks lacking KAISO; REST&KAISO – methylation of REST motifs of peaks containing both REST and KAISO motifs; KAISO – methylation of KAISO motifs present in REST ChIP-seq peaks with identified KAISO but not REST motif; KAISO&REST – methylation of KAISO motifs of peaks containing both REST and KAISO motifs.

(B) DNA methylation of REST or KAISO motifs within the REST ChIP-seq peaks assigned to REST-activated targets. Description as in (A).

(C) Distribution of REST motif DNA methylation in the REST ChIP-seq peaks containing only REST motifs and assigned to the repressed or activated REST targets.

(D) Distribution of REST motif DNA methylation in the REST ChIP-seq peaks containing both REST and KAISO motifs and assigned to the repressed or activated targets**.**

(E) Cumulative distribution of DNA methylation in individual motifs. There are 601 sites containing REST or KAISO motifs with significantly different methylation among gliomas.

(F-G) Human disease pathways **(F)** and REACTOME pathways **(G)** enriched among 47 REST targets. REST-ChIP-seq peaks assigned to these targets had at least one differentially methylated REST or KAISO motif.

(H) Distribution of DNA methylation of REST or KAISO motifs within REST ChIP-seq peaks assigned to the genes present in enriched pathways - shown in (F) and (G).

(I) Correlation between expression of a REST-target gene and mean DNA methylation of a motif assigned to its promoter. Correlations were performed using the Glioma Atlas dataset. Black squares mark REST-targets having REST and KAISO motifs in the REST ChIP-seq peaks, while white squares mark those in which only REST motifs were detected.

(J) Correlation between expression of a REST-target gene and mean DNA methylation of its promoter. Analyses performed using the data from TCGA dataset.

The number sites with predicted REST and/or KAISO motifs within a single REST-peak was high, which did not allow for unequivocal determination which of predicted motifs was actually used for TF binding. Thus, we studied DNA methylation patterns within individual motifs for the REST or KAISO TFs across gliomas using the DiffMeth tool and methylomes of GII/GIII IDH-WT, GII/GIII/GIV IDH-MUT and GIV IDH-WT gliomas from the Glioma Atlas (Stępniak et al., 2021). Initially, over 70,000 REST and KAISO motif sites were found within REST-ChIP-seq peaks of glioma cells (Table S2), and 601 of them were differentially methylated among gliomas, which accounts for 0.9% of the all identified REST and KAISO motif sites (Figure 6E). The proportion between all predicted sites of individual motifs compared to a number of differentially methylated sites was significantly different (p-value < 0.01, Table S2). We identified six of the twelve REST motifs as having differential DNA methylation in gliomas (Table S2) and a majority of differentially methylated sites of REST motifs were found within REST-ChIP-seq peaks corresponding to REST-repressed targets (X-squared = 97.069, df = 13, p-value = 6.119e-15).

Differentially methylated sites (n=601) among gliomas had the highest median β-value in IDH-MUT and the lowest in GIV gliomas (Figure 6E). Frequently, more than one motif showed significantly differential methylation in a single REST ChIP-seq peak. We found that sites differentially methylated in gliomas appeared within 47 REST-ChIP-seq peaks, out of which 32 were associated with REST-repressed targets, while 15 with REST-activated targets. A complete list of REST targets paired with the REST-ChIP-seq peaks containing differentially

methylated REST or KAISO motif sites is presented in the Table S3. For these genes, we searched for associations with diseases using the DisGeNET platform and enrichment of specific biological pathways using the REACTOME database. Nine out of 47 genes were linked to disorders, including epilepsy, encephalopathies, and febrile convulsions (Figure 6F). Nine genes were associated with significantly enriched REACTOME pathways (Figure 6G). The largest number of genes (n=5), all under REST repression, were linked with L1 cell adhesion molecule (L1CAM) interactions. Several genes (n=6), all assigned as REST-repressed targets, were linked to another three pathways: recycling pathway of L1, gap junction trafficking and regulation, and potassium channels (Figure 7G). We found that the biological functions associated with L1CAM interactions and cell differentiation (*RUNX2* regulates osteoblast differentiation) are similar to pathways detected to be altered in IDH-WT and IDH-MUT REST depleted cells (Figure 3). Some of the genes defined as REST-activated targets (namely, *NTF3* and *GLI3*) and the genes containing KAISO motifs within the REST ChIP-seq peaks (namely *GLI3, NTF3, HCN2, SCN3B* and *SLC8A2*) had a methylation pattern similar to the repressed REST targets (Figure 6H).

To verify whether differentially methylated motif sites affect expression of REST targets, we calculated correlation between mean methylation and gene expression using the Glioma Atlas (Figure 6I) and TCGA datasets (Figure 6J). The methylome data in the Glioma Atlas are dense, thus we were able to calculate TF motif site mean methylation and correlate it with REST target expression. Correlations were also performed on TCGA data to validate the results obtained on the Glioma Atlas, but due to low number of cytosines covered, mean methylation was computed for the entire promoters. Expression of most REST activated targets negatively correlated with site/promoter methylation levels. Interestingly, for the repressed genes, the positive correlation was more frequently detected (Figure 6I-J). The correlation results obtained on the Glioma Atlas data demonstrate that a negative correlation coefficient corresponds well with KAISO motif presence in a ChIP-seq peak assigned to a gene (Figure 6I black squares) and a negative correlation with its absence (Figure 6I white squares).

REST gene targets affected by REST knockdown belong to cell migration and differentiation pathways

REST knockdown may directly affect genes that are activated or repressed by REST binding (hereafter primary REST targets). REST knockdown may also have indirect effects related to altered interactions between REST and other proteins and/or downstream regulatory cascades released by primary REST targets (hereafter REST secondary targets). To separate primary from the secondary REST targets, the genes significantly affected by REST knockdown were intersected with genes assigned to REST ChIP-seq peaks. GO Biological Pathways enriched among the genes up-regulated in REST depleted cells and having REST binding at their promoters' comprised pathways related to neuronal transmission (signal release, calcium regulated exocytosis), and glial cell migration (Figure 7A, upper panel). The pathways related to the genes down-regulated in REST depleted cells and whose promoters showed REST binding, included NAD biosynthetic process, regulation of mRNA splicing and hematopoietic progenitor cell differentiation (Figure S3B).

Further, a correlation of REST and its targets expression was calculated in the TCGA dataset. A majority of the genes enriched in the signal release, calcium regulated exocytosis and telencephalon glial cell migration biological pathways in REST depleted cells (Figure 7A) was similarly regulated in GIV gliomas (Figure S3A). Nearly half of the down-regulated genes

in REST depleted cells related to NAD biosynthetic process, regulation of mRNA splicing and hematopoietic progenitor cell differentiation (Figure 7A), showed similar pattern in GIV gliomas (Figure S3B). Most of the genes up-regulated in the cells with REST knockdown were consistently down-regulated in gliomas compared to normal brain, with expression decreasing in the direction from WHO grades II and III to GIV (Figure 7B). Genes down-regulated in REST depleted cells did not show this pattern in TCGA gliomas (not shown). Correlation of the REST up- or down-regulated genes with glioma cellular states described by Neftel et al. 2019 showed that many of the genes correlated with cellular states that recapitulate neural progenitor-like (NPC-like), oligodendrocyte progenitor-like (OPC-like), astrocyte-like (AC-like) or mesenchymal-like (MES-like) states and/or states characteristic for cycling cells related to G1S or G2M cell cycle transition phases (Figure 7C). Many genes up-regulated in REST depleted cells show significant positive correlation with NPC-like states and a negative correlation with G1S and G2M states, suggesting rather non-cycling cells (Figure 8C). Finally, the genes up-regulated in REST depleted U87 glioma cells show a concordance of their REST binding sites with these detected directly from glioma tumors, collected within the study (Figure 7D), which was not the case among genes down-regulated in REST depleted cells (not shown).

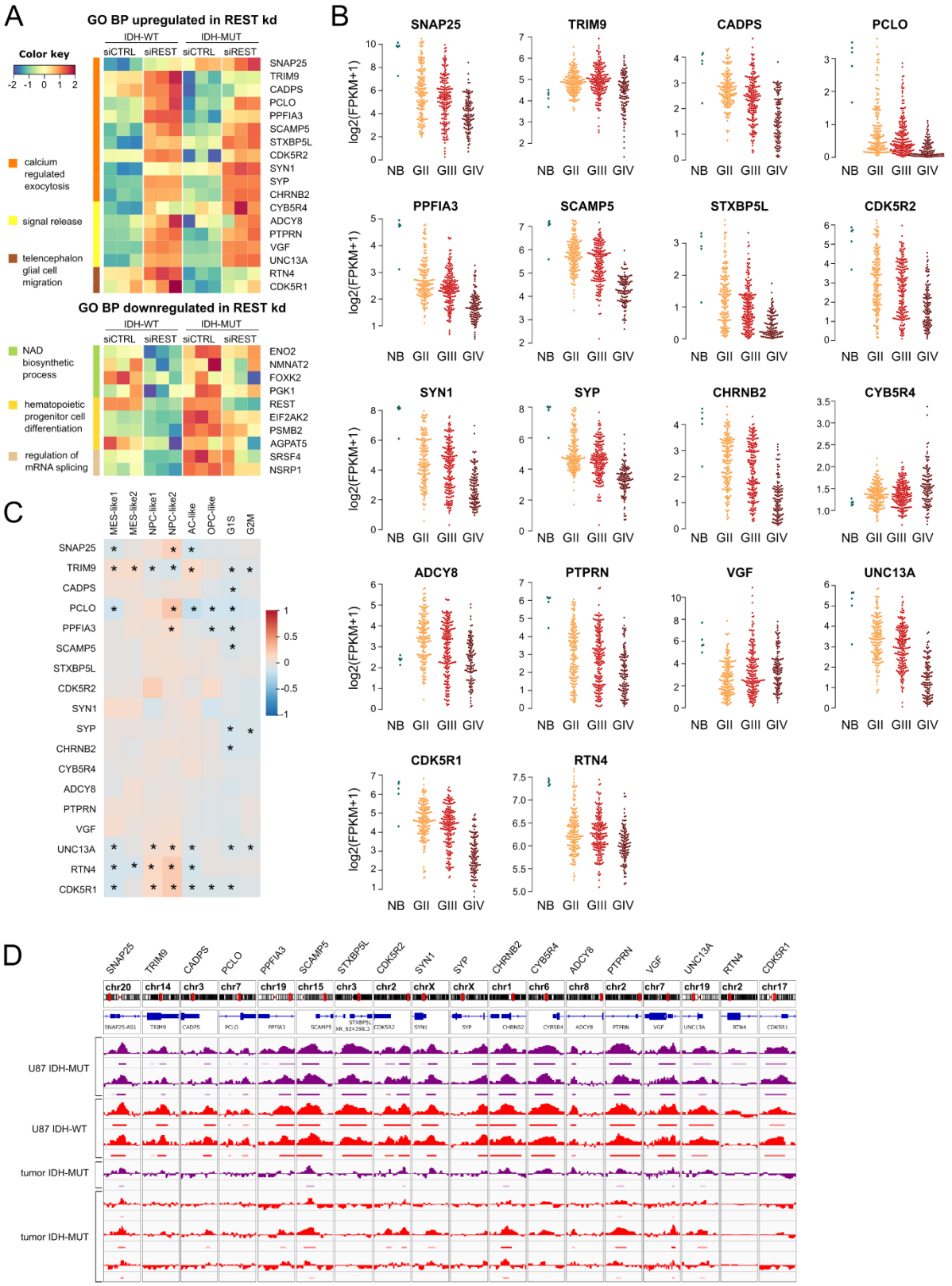

Figure 7. Genes affected by REST knockdown and having REST ChIP-seq peaks belong to migration and differentiation pathways.

(A) Upper panel: top GO BP pathways up-regulated in REST depleted cells and defined as REST targets in ChIP-seq experiments were related to calcium release exocytosis, signal release and encephalon glial migration pathways. Lower panel: Main GO BP pathways down-

regulated in REST depleted cells and defined as REST targets in ChIP-seq experiments were related to: NAD biosynthetic process, hematopoietic progenitor cell differentiation and regulation of mRNA splicing pathways.

(B) Expression of genes up-regulated in REST depleted cells (from panel A) in TCGA LGG/GBM datasets and presented as beeswarm plots for NB (normal brain), glioma WHO grade II, III and IV.

(C) Expression of genes up-regulated in REST depleted cells was correlated in single cell RNAseq data with cellular states defined by Neftel et al 2019. Pearson correlation was calculated, and a color key scale was used to present its values in range of -1 to 1, correlation significance was marked (*) when adjusted $p<0.05$.

(D) Genomic view from Integrative Genome Viewer on genes up-regulated in REST depleted cells and gliomas for each sample a histogram of reads was normalized to the input reads (bigwigg file) and bed file from ChIP-seq experiment was shown. REST ChIP-seq data on four U87 glioma cell repetitions (2x IDH-MUT and 2x IDH-WT) and 4 tumor samples (1x IDH-MUT and 3x IDH-WT) are shown. IDH-MUT samples are color-coded in purple and IDH-WT in red.

Discussion

We performed a comprehensive study identifying transcriptional targets of REST transcription factor and complete REST regulatory networks in glioma cells with a different IDH status. These findings were validated in gliomas of different malignancy and public TCGA datasets. Using a large spectrum of computational methods, ChIP-seq, RNA-seq, DNA methylation and RNAi mediated REST knockdown in U87 cells with a wild type or mutant *IDH1*, we addressed a complex role of REST in gliomagenesis. Recognition of the importance of IDH1/2 mutations in progression of diffuse gliomas advanced our understanding of glioma biology, however the full impact of a state of DNA and histone hypermethylation, leading to the CpG island methylator phenotype, on gene regulatory networks and cell functions is less clear. Our study demonstrates that REST-regulated gene networks in gliomas are dependent on the *IDH* mutation status, which determines a selection of REST dependent genes involved in ECM organization, glioma invasion and cell differentiation. We uncovered a putative cooperation between REST and KAISO in determining REST target repression or activation. Our results point to REST as a valid target in anti-glioma therapy.

Exploration of TCGA datasets showed increased *REST* expression in malignant gliomas, and in IDH-mutant gliomas. High *REST* expression has been reported as a negative prognostic factor for survival in GBM (Liang et al., 2016) and medulloblastoma patients (Taylor et al., 2012a). In mice, expression of REST in glioma stem cells (GSCs) was negatively correlated with survival and considered as a critical factor in maintenance of their self-renewal (Kamal et al., 2012). While in a joint cohort of lower grade gliomas and GBM *REST* expression was inversely correlated with patients survival as previously reported (Conti et al., 2012; Kamal et al., 2012; Wagoner and Roopra, 2012), we found that its high expression is an unfavorable prognostic factor in LGG with the *IDH* mutation, but a favorable factor in GBM (Figure 1). Finding a positive correlation of *REST* expression with survival of GBM patients appears surprising and requires more studies.

Several studies reported that REST acts as an oncogene in gliomas, promoting cell proliferation and invasion (Conti et al., 2012; Kamal et al., 2012). REST expression was associated with high tumor aggressiveness and invasiveness, as well as chemotherapy resistance (Conti et al., 2012; Kamal et al., 2012; Wagoner and Roopra, 2012). However, the

underlying gene regulatory networks have not been elucidated yet. REST knockdown in U87 glioma cells affected many biological pathways. Numerous genes linked to neuronal functioning were up-regulated, while genes linked to cell proliferation were down-regulated in REST depleted cells, regardless of the *IDH* status (Figure 2F). However, a large subset of DEGs between IDH-WT and IDH-MUT glioma cells were differently affected by REST knockdown (Figure 3A). We found those genes belonged to GO biological processes related to ECM organization and glial/neuronal cell differentiation. Contrary to Zhang et al observations (Zhang et al., 2016), REST knockdown did not affect cell viability in our model, but it did influence cell invasiveness in IDH phenotype-specific manner. We also observed much higher invasion of the IDH-MUT compared to IDH–WT cells. These observations raised a question on how the changes in DNA methylation resulting from the *IDH* mutation affect REST targets and processes in which they are involved.

Using U87 IDH-WT and IDH-MUT isogenic cell lines allowed us to address the issue of how DNA hypermethylation affects sets of REST regulated genes. REST-ChIP-seq data on human glioma cells integrated with the results of transcriptomic changes in REST depleted cells allowed a precise defining direct and indirect REST targets. Scrutinizing REST-ChIP-seq peaks we found REST binding motifs co-occurring with the binding sites for other TFs, among which KAISO was identified as an important partner in gene regulation. Interestingly, depending on the co-occurrence of REST and KAISO binding sites the effects on transcription varied and different GO biological pathways were found to be regulated. We confirmed that genes selected as REST targets in cultured glioma cells, were co-expressed in a REST dependent manner in TCGA glioma datasets.

The identified REST gene regulatory networks and biological functions agree with observations of a key role of REST as a repressor of genes involved in cell differentiation. REST depletion promotes neuronal differentiation (Lee et al., 2016), and can regulate the timing of neural progenitor differentiation during neocortex development (Mandel et al., 2011). The evidence of REST involvement in cell migration and invasion is ambiguous. On one hand, REST blocks NPC radial migration during neurogenesis (Mandel et al., 2011) and acts as cell migration repressor in microglia (Yu et al., 2020). However, medulloblastoma cells overexpressing REST migrated faster in wound-healing assay compared to controls (Callegari et al., 2018). Downregulation of REST in glioblastoma cells inhibited cell migration and proliferation (Zhang et al., 2016). In our dataset we did not observe change in cell proliferation, but we observed that IDH-MUT glioma cells are considerably more invasive (Figure 4C), which is consistent with data on IDH-MUT tumors (Huang et al., 2019; van Lith et al., 2014; Pientka et al., 2012). In this study, REST knockdown increased expression of ECM related genes (Figure 4A) and invasion of IDH-MUT glioma cells (Figure 4C) This coincided with changes in promoter and gene body methylation in more than half of the cases (Figure 4D, E). We propose that REST-regulated genes from the ECM related biological pathway could contribute to the increased invasiveness of IDH-MUT gliomas.

The analysis of the REST-binding sites in ChIP-seq peaks shed light on different REST activity depending on the IDH status. The differences in the number of ChIP-seq peaks (Figure 5A) and in genomic distribution of DNA binding sites (Figure 5B) between IDH-WT ad IDH-MUT suggest a stronger transcriptional regulation by REST (including both, repression, and activation) in IDH-WT glioma cells. Some genomic locations of REST ChIP-seq peaks were exclusive to IDH-WT or IDH-MUT cells, further adding up to the possible differences in REST regulation in IDH-WT and IDH-MUT. Moreover, the REST ChIP-seq peaks in IDH-WT and IDH-MUT cells contained differing sets of other transcription factor binding motifs (Figure S4). Different composition of other TF motifs was also detected between peaks assigned to REST-

repressed and -activated targets. (Figure 5 and S6) suggesting differences in gene regulation by specific factors (Darieva et al., 2010; Gurdon et al., 2020; Zabet and Adryan, 2013). Increased *REST* expression in GIV gliomas and decreased in IDH mutant gliomas may result in REST binding to the sites that are otherwise occupied by other TFs with a different mode of action. Potential competitors of REST in regulation of its targets in IDH-WT and IDH-MUT cells included KAISO (ZBTB33), a methylation-sensitive TF (Daniel et al., 2002; Prokhortchouk et al., 2001).

KAISO is a transcriptional repressor acting as either a tumor suppressor or oncogene in various human cancers (Pierre et al., 2019a). We found that KAISO TF motifs discriminate between the REST binding sites specific for IDH-WT and IDH-MUT cells. All three KAISO motifs were found in a number of REST ChIP-seq peaks specific for IDH-WT and common for both IDH-MUT and IDH-WT cells. Contrary, not a single KAISO motif was detected among the motifs present in the REST ChIP-seq peaks specific for IDH-MUT cells (Figure S4). Depending on the co-occurrence of REST and KAISO binding sites, the effects on transcription and DNA methylation patterns varied (Figures 6A-E, 6G, 7E, 7F) and different GO biological pathways were found to be regulated (Figure S6). In addition, the KAISO-binding motif 2.A, which is bound by KAISO when unmethylated, was among the top motifs found in REST-activated but not in REST-repressed genes (Figure 4C, G). While repressive role of REST has been well documented, its role in gene activation is less described and our findings contribute to understanding of this topic. REST gene activation in glioma cells is consistent with previous findings indicating that REST splice isoform REST4 activates gene expression in neural cells (Abramovitz et al., 2008). Possibly, the glioma cells may hijack this neuronal cell's specific regulation for their own purposes. One possible mechanism that has to be further elucidated is related to DNA methylation, which has atypical relationship with targeted gene expression. Our findings suggest that REST activated genes promoters' methylation may be positively correlated with their expression, in contrast to a common view (Figure 6 I,J). An example of enhancing of REST binding by DNA methylation was demonstrated in developing mouse hearts, but that case was connected to gene repression (Zhang et al., 2017).

Intersection of the genes with assigned REST ChIP-seq peaks with those affected by REST knockdown uncovered a number of genes that are high confidence primary targets of REST (Figure 7). Among genes up-regulated in REST depleted cells we found genes related to signal release, calcium regulated exocytosis and telencephalon glial cell migration as identified with the REACTOME enrichment analysis. Most of these genes showed decreased expression in GII and GIII gliomas compared to normal brain, with the lowest expression in GIV gliomas (Figure 7B). The expression of these genes was negatively correlated with signatures of G1S and G2M phases of the cells cycle, and positively correlated with NPC-like cellular states as defined by Neftel et al 2019. As NPC-like cellular states are enriched in the proneural GBM (Neftel et al., 2019), originally defined as IDH-MUT GBMs or secondary GBMs (Verhaak et al., 2010), our findings suggest that REST plays a role specifically in these malignant gliomas. Intermediate expression of *REST* in GII/III gliomas (Figure 1A) may be enough to maintain a higher expression of the genes contributing to the NPC-like state. High *REST* expression in GIV gliomas might be associated with a strong repression of these genes. This could explain why while REST is a negative prognostic factor in GII/III gliomas, it a positive factors in GIV.

In summary, we identified REST targets, gene regulatory networks and putative REST cooperativity with other TFs that differentially control gene expression in IDH-WT and IDH-MUT gliomas. Among REST targets we found genes involved in glial cell differentiation and ECM organization. Knockdown of REST had different impact on glioma invasion depending

on the IDH phenotype, which is connected to DNA hypermethylation phenotype. We demonstrate that REST–mediated gene transcription activation or repression might be differentially modulated by DNA methylation and by cooperation/competition with other transcription factors, such as KAISO (ZBTB33). The DNA methylation of REST activated genes often showed a positive correlation with gene expression, suggesting that hypermethylation phenotype of IDH-MUT may have a strong impact on these genes. Finally, repression of the canonical REST gene targets may play a more significant role in IDH-MUT grade II/III gliomas than in GIV gliomas by maintaining NPC-like cellular state properties. Therefore, REST could be considered as a crucial factor in the design of targeted glioma therapies.

STAR METHODS

KEY RESOURCES TABLE

REAGENT or RESOURCE	SOURCE	IDENTIFIER
Antibodies		
Rabbit anti-REST antibody	Millipore	CS200555
Mouse anti-GAPDH antibody	Millipore	MAB374
Rabbit IgG antibody	Millipore	PP64B
Horseradish peroxidase-conjugated anti-β-actin antibody	Sigma	A3854
Horseradish peroxidase- conjugated anti-rabbit IgG	Vector	PI-1000
Chemicals		
Human REST-targeting siRNA ON-TARGETplus SMARTpool	Dharmacon	L-006466-00-0005
Human control siRNA ON-TARGETplus SMARTpool	Dharmacon	D-001810-10-05
AMPure XP Beads	Beckman Coulter, Brea, California, US	A63881
Poly-T oligo-attached magnetic beads	Kapa Biosystems, MA, USA	
Agarose beads protein G	Invitrogen	
Agarose beads protein A	Invitrogen	
Cozy prestained protein ladder	High Qu GmbH	PRL0102c1
DMEM medium	Gibco	31885-023
FBS	PAN-BIOTECH, South America	P30-3302
Lipofectamine 2000	Invitrogen	2094065
PrestoBlue™ Cell Viability reagent	Invitrogen	A13262
Chemiluminescence detection	BioRad	

system (ECL)		
Growth Factor Reduced Matrigel™ Matrix	BD Biosciences	356231
VECTASHIELD Antifade Mounting Medium with DAPI	Vector Laboratories, USA	H-1800
SuperScript III Reverse Transcriptase	Invitrogen, USA	18080-044
Fast Sybr Green Master Mix	Applied Biosystem by Thermo Fisher Scientific	4385612
Critical commercial assays		
SE Cell line Solution box	Lonza	PBC1-02250
KAPA Stranded mRNAseq Kit	Roche Diagnostics, Basel, Switzerland	07962193001
Qiaseq Ultralow Input Library Kit	Qiagen, Hilden, Germany	ZZ-QG-180492
Agilent 6000 RNA Pico Kit	Agilent Technologies, Santa Clara, California, US	5067-1513
Agilent HS DNA Kit	Agilent Technologies, Santa Clara, California, US	5067-4626
Quanti Fluor ONE dsDNA Kit	Promega, Madison, Wisconsin, US	E4870
RNeasy Mini Kit	Qiagen, Hilden, Germany	74106

Deposited data		
The Cancer Genome Atlas	https://portal.gdc.cancer.gov/	GBM and LGG
Human glioma samples, glioma Atlas	Data covering transcriptomes and methylomes of various glioma grade tumors: IDH-MUT, IDH-WT, GIV is available at the resource website: http://regulomics.mimuw.edu.pl/GliomaAtlas Glioma Atlas have been deposited in the European Nucleotide Archive	ERP125425
Transcription factor position weight matrices from HOCOMOCO database	HOCOMOCO: towards a complete collection of transcription factor binding models for human and mouse via large-scale ChIP-	https://hocomoco11.autosome.ru/downloads_v11

	Seq analysis, Ivan V. Kulakovskiy; Ilya E. Vorontsov; Ivan S. Yevshin; Ruslan N. Sharipov; Alla D. Fedorova; Eugene I. Rumynskiy; Yulia A. Medvedeva; Arturo Magana-Mora; Vladimir B. Bajic; Dmitry A. Papatsenko; Fedor A. Kolpakov; Vsevolod J. Makeev, Nucl. Acids Res., Database issue, gkx1106 (11 November 2017), doi: 10.1093/nar/gkx1106	
REST transcription factor position weight matrices from ENCODE database	https://www.nature.com/articles/nature28170#Sec2 http://compbio.mit.edu/encode-motifs/ motywy, mają te same nazwy co te, które mi wysłałeś, więc proponuję podać to "Systematic discovery and characterization of regulatory motifs in ENCODE TF binding experiments"	
Classification of Transcription Factors in Mammalia from HOCOMOCO database	HOCOMOCO: towards a complete collection of transcription factor binding models for human and mouse via large-scale ChIP-Seq analysis, Ivan V. Kulakovskiy; Ilya E. Vorontsov; Ivan S. Yevshin; Ruslan N. Sharipov; Alla D. Fedorova; Eugene I. Rumynskiy; Yulia A. Medvedeva; Arturo Magana-Mora; Vladimir B. Bajic; Dmitry A. Papatsenko; Fedor A. Kolpakov; Vsevolod J. Makeev, Nucl. Acids Res., Database issue, gkx1106 (11 November 2017), doi: 10.1093/nar/gkx1106	https://hocomoco11.autosome.ru/human/mono?full=true

Experimental Models: Cell culture		
U87-MG	American Type Culture Collection	HTB-14 IDH-WT
U87-MG-IDH-MUT	American Type Culture Collection	HTB-14IG

Software and Algorithms		
CytoMeth	WIll be published separately as a tool	https://github.com/mdraminski/CytoMeth
DiffMeth	This paper	https://github.com/mdraminski/transcripionFactorREST
PWMEnrich	N/A	https://bioconductor.org/packages/release/bioc/html/PWMEnrich.html (v4.20)
FIMO tool from MEME Suite	FIMO: Scanning for occurrences of a given motif, Charles E. Grant, Timothy L. Bailey and William Stafford Noble, Bioinformatics 27(7):1017-1018, 2011.	https://meme-suite.org/meme/tools/fimo (v5.3.0)
Centrimo tool from MEME Suite	Inferring direct DNA binding from ChIP-seq, Timothy L. Bailey and Philip Machanick, Nucleic Acids Research, 40:e128, 2012.	https://meme-suite.org/meme/tools/centrimo (v5.4.1)
VennDiagram	N/A	https://cran.r-project.org/web/packages/VennDiagram/index.html (v1.6.20)
phylotools	phytools: an R package for phylogenetic comparative biology (and other things), Liam J. Revell, Methods in Ecology and Evolution2012,3, 217–223, doi: 10.1111/j.2041-210X.2011.00169.x	https://cran.r-project.org/web/packages/phytools/index.html (v1.0-1)
seqLogo	N/A	https://bioconductor.org/packages/release/bioc/html/seqLogo.html (v.1.50.0)
STAMP	DNA familial binding profiles made easy: comparison of various motif alignment and clustering strategies, S Mahony, PE Auron, PV Benos, PLoS Computational Biology (2007) 3(3):e61	http://www.benoslab.pitt.edu/stamp/

Graph Pad Prism	http://www.graphpad.com	
ImageJ	http://www.imagej.net	
biomaRt	Durinck S, Spellman P, Birney E, Huber W (2009). "Mapping identifiers for the integration of genomic datasets with the R/Bioconductor package biomaRt." *Nature Protocols*, **4**, 1184–1191.	https://bioconductor.org/packages/release/bioc/html/biomaRt.html (version 2.40.5), dataset="hsapiens_gene_ensembl",host='jul2018.archive.ensembl.org'
beeswarm plot	N/A	https://www.rdocumentation.org/packages/beeswarm/versions/0.4.0/topics/beeswarm
corrplot	N/A	https://www.rdocumentation.org/packages/corrplot/versions/0.92 (version 0.84)
plotly	N/A	https://www.rdocumentation.org/packages/plotly/versions/4.10.0 (version 4.9.1)
DESeq2	Love MI, Huber W, Anders S (2014). "Moderated estimation of fold change and dispersion for RNA-seq data with DESeq2." Genome Biology, 15, 550. doi: 10.1186/s13059-014-0550-8.	https://bioconductor.org/packages/release/bioc/html/DESeq2.html (version 1.24.0)
ggrepel	N/A	https://www.rdocumentation.org/packages/ggrepel/versions/0.9.1 (version 0.8.1)
clusterProfiler	Wu T, Hu E, Xu S, Chen M, Guo P, Dai Z, Feng T, Zhou L, Tang W, Zhan L, Fu x, Liu S, Bo X, Yu G (2021). "clusterProfiler 4.0: A universal enrichment tool for interpreting omics data." The Innovation, 2(3), 100141. doi: 10.1016/j.xinn.2021.100141	https://bioconductor.org/packages/release/bioc/html/clusterProfiler.html (version 3.12.0)
org.Hs.eg.db	N/A	https://bioconductor.org/packages/release/data/annotation/html/org.Hs.eg.db.html (version 3.8.2)

ggplot2	N/A	https://www.rdocumentation.org/packages/ggplot2/versions/3.3.5 (version 3.3.5)
plotrix	N/A	https://www.rdocumentation.org/packages/plotrix/versions/3.8-2 (version 3.7-7)
TxDb.Hsapiens.UCSC.hg38.knownGene	N/A	https://bioconductor.org/packages/release/data/annotation/html/TxDb.Hsapiens.UCSC.hg38.knownGene.html (version 3.4.6)
ChIPseeker	Yu G, Wang L, He Q (2015). "ChIPseeker: an R/Bioconductor package for ChIP peak annotation, comparison and visualization." Bioinformatics, 31(14), 2382-2383. doi: 10.1093/bioinformatics/btv145.	https://bioconductor.org/packages/release/bioc/html/ChIPseeker.html (version 1.20.0)
survival		https://cran.r-project.org/web/packages/survival/index.html (version 2.44)
survminer		https://cran.r-project.org/web/packages/survminer/index.html (version 0.4.8)
ggtree	Using ggtree to Visualize Data on Tree-Like Structures, Yu G, Current Protocols in Bioinformatics, 69(1), e96. doi: 10.1002/cpbi.96, 2020	https://bioconductor.org/packages/release/bioc/html/ggtree.html (v1.16.6)
bedtools		https://bedtools.readthedocs.io/en/latest/

RESOURCE AVAILABILITY

Lead contact

Further information and requests for resources and reagents should be directed to and will be fulfilled by the Lead Contact, Bartosz Wojtas (b.wojtas@nencki.edu.pl).

Materials availability

This study did not generate new unique reagents.

Data and Code Availability

- RNAseq and ChIPseq data generated in this study have been deposited to the GEO (Gene Expression Omnibus) data repository and are located in directories under the following ID: GSE174308.
- Availability of tumor methylome and transcriptome data (here after glioma Atlas, Stępniak et al.2021) is regulated by material transfer agreements with the scientists creating the methylome and transcriptome data.
- This paper also analyzes existing, publicly available data. These data sets' accession numbers are provided in the Key Resources table.
- Additional scripts used to generate figures and computational analysis reported in this paper are available at Github (https://github.com/mdraminski/transcriptionFactorREST).
- Any additional information required to reproduce this work is available from the Lead Contact.

EXPERIMENTAL MODEL AND SUBJECT DETAILS

Cell culture

The experiments were conducted using U87-MG (ATCC HTB-14 IDH-WT) and IDH1 mutant-U87 Isogenic Cell Line (ATCC HTB-14IG), purchased from American Type Culture Collection (ATCC). The cells were cultured in DMEM (Gibco), 10% FBS (PAN-BIOTECH) with no antibiotics added. Cells were passaged every 3-5 days depending on the seeding density.

Human glioma samples

This study used glioma tumor data generated in the work of Stepniak et al, 2021 https://pubmed.ncbi.nlm.nih.gov/34131149/ (EGA accession nr: ERP125425)

REST-ChIP-seq in human glioma samples

Glioma tumors (n=7) REST- ChiP-seq results were obtained with a protocol described in Stepniak et al, 2021 (https://pubmed.ncbi.nlm.nih.gov/34131149/) with the exception of using REST antibody (Millipore) instead of a histone mark antibody.

Human glioma samples: methylomes

5mC DNA methylation data (NimbleGen SeqCap Epi from ROCHE) include glioma tumor samples of WHO grade II/III IDH-WT (n=4), grade IV IDH-WT (n=11) and four IDH-MUT samples (n=4), obtained from the recently published atlas of active enhancers and promoters in benign and malignant gliomas (Stepniak et al., 2021). In our study we refer to this dataset as "glioma Atlas". All four IDH-MUT samples were pooled together and hereafter are referred to as IDH-MUT. The glioma Atlas data covers millions of cytosines in a base pair resolution. Due to tumor-related DNA degradation, methylomes presented in the Atlas consist of over 10 million of cytosines per sample on average. Despite the limited number of tumor type specific

samples, the number of covered DNA sites in the Atlas is a huge advantage in comparison to BeadChip panels such as Infinium® HumanMethylation450 or MethylationEPIC performed on larger patient cohorts.

Human glioma samples: RNA-seq

RNA-seq row counts of genes were obtained for the same set of samples from the glioma Atlas whose methylomes were analyzed (n=4 IDH-MUT, n=4 IDH-WT LGG, n=11 IDH-WT GIV)..

TCGA public data

TCGA level 3 RNA-seq data (aligned by STAR and gene expression counted by HTseq) were uploaded to R. Data from TCGA GBM (glioblastoma, WHO grade IV) and LGG (lower grade gliomas, WHO grade II/III) repositories were uploaded. Gene expression levels as FPKM (fragments per kilobase of exon per million) were used for further analysis of REST expression in the context of glioma malignancy grades and IDH1/2 mutation status. Clinical data for LGG and GBM datasets were obtained from the work of Ceccarelli et al. 2016 (Table S1 therein).

Single cell RNA-seq data

Glioma tumor samples scRNA-seq data (Neftel et al 2019) were uploaded from GEO (GSE131928) and data were uploaded to R as TPM values.

METHOD DETAILS

siRNA-REST knockdown

REST knockdown was performed in isogenic malignant glioma cell lines that genetically differed by IDH1 mutation status (hereinafter referred to as U87-WT and U87-MUT). The cells were subcultured 2 days prior to the transfection so they would not exceed the confluency of 80% on the day of siRNA transfection. For the nucleofection, cells were trypsinized, counted, centrifuged, resuspended in Lonza SE cell line solution reagent and transferred to Nucleocuvette Vessel (Lonza). Control or human REST-targeting siRNA ON-TARGETplus SMARTpool (Dharmacon) was then added to the appropriate wells of the vessel and nucleofection was carried out using 4D-Nucleofector core unit. The cells were then resuspended with DMEM 10% FBS and cultured in 12 or 24 well plates (Falcon) for the next 24 hours. After that time the medium was replaced with fresh DMEM 10% FBS and the cells were transfected for the second time using Lipofectamine 2000 (Invitrogen, 2094065) and the same siRNA ON-TARGETplus SMARTpool (Dharmacon) as before. Protein and RNA were collected 72 hrs after the first transfection.

RNA isolation

RNA was isolated from U87-WT and U87-MUT cells that were either not treated or transfected with control or REST-targeting siRNA. RNeasy Mini Kit (QIAGEN) was used according to the producer's protocol. RNA concentration was measured with NanoDrop 2000 (Thermo Scientific, NanoDrop products, Wilmington, USA). RNA quality was verified with Bioanalyzer

2100 (Agilent Technologies, Santa Clara, CA) using an RNA 6000 Nano Kit (Agilent Technologies, Ltd.).

Quantitative PCR (qRT-PCR)

Total RNA was extracted from glioma cells using the RNeasy Mini kit (Qiagen, Hilden, Germany) and purified using RNeasy columns according to the manufacturer's instructions. cDNA was synthesized by extension of oligo(dT) primers with SuperScript III Reverse Transcriptase (Invitrogen, USA). Real-time PCR was performed applying SYBR Green chemistry (Cat. Number 4385612, Applied Biosystem by Thermo Fisher Scientific) on QuantStudio 12 K Flex Real-Time PCR System device using primers indicated in Key Sources Table. Amplified product was normalized to the endogenous expression of GAPDH and represented as -ΔΔCt (negative delta delta Ct) values (fold change). Statistical significance of comparisons between groups was calculated in GraphPad Prism v. 9.1.2 (GraphPad Software, LCC). P values were considered significant when *P < 0.05 (Mann-Whitney test).

Western Blotting

Whole-cell protein extracts were prepared, resolved by electrophoresis and transferred to a nitrocellulose membrane (GE Healthcare cat. number 10600003) as described (Ciechomska et al., 2003). After blocking with 5% non-fat milk in TBST (Tris-buffered solution pH 7.6, 0.01% Tween-20) the membranes were incubated overnight with primary antibody (rabbit anti-REST1, 1:1000; Millipore or mouse anti-GAPDH, 1:500, Millipore MAB374) in TBST with 5% bovine serum albumin (BSA) or 1 h with horseradish peroxidase-conjugated anti-β-actin antibody (Sigma cat. number A3854) diluted 1:20000 in 5% non-fat milk in TBST. The primary antibody reaction was followed by 1 h incubation with horseradish peroxidase- conjugated anti-rabbit IgG diluted at 1:10000 (Vector cat. number PI-1000). Immunocomplexes were detected with an enhanced chemiluminescence detection system (ECL) and Chemidoc (Biorad). The molecular weight of proteins was estimated with Cozy prestained protein ladder (High Qu GmbH cat. number PRL0102c1). Densitometry of band intensities was performed using BioRad Image Lab software. REST band intensities were normalized to GAPDH band intensities for each blot. Statistical significance of comparisons between groups was calculated in GraphPad Prism v. 9.1.2 (GraphPad Software, LCC). P values were considered significant when *P < 0.05 (column statistics t-test).

PrestoBlueTM Cell Viability assay

PrestoBlue™ Cell Viability reagent (Invitrogen) is quickly reduced by metabolically active cells resulting in its color change, providing a quantitative measure of cell viability. In this assay we used blank (no cells), not treated, mock transfected and siRNA-transfected U87-WT and U87-MUT cells. Transfection was carried out as described earlier (nucleofection followed by lipofection). Cells were seeded at 24 well plates at 40k/well. Time points for measuring the viability were 12h, 24h, 48h and 72h post nucleofection. PrestoBlueTM Cell Viability reagent (10x concentrated, Invitrogen) was added for 30 minutes incubation in 37℃ (with gentle shaking) at a final concentration of 1x. A portion of PrestoBlue diluted in the medium was kept at the same conditions to be used as a blank. After incubation, 100ul of medium was transferred from theto 96 well plates and the fluorescence was read at an excitation/emission

wavelength of 560/590 nm using BioTek Synergy HTX fluorimeter. Data was analyzed in GraphPad Prism using Wilcoxon matched-pairs signed rank test, two-tailed. For each timepoint, mock transfected cells viability was normalized to 100%.

Matrigel Invasion assay

Matrigel invasion assay was performed using tissue culture inserts (6.5 mm Transwell® with 8.0 µm Pore Polycarbonate Membrane Insert, Corning, NY) coated with the Growth Factor Reduced Matrigel™ Matrix (BD Biosciences). 50 µL of the Matrigel™ Matrix (1 mg/mL) diluted in fresh DMEM medium was dried under sterile conditions (37°C) for 4.5-6 h. The medium was added to the wells 1 h before seeding the glioma cells into inserts. The U87-WT and U87-MUT cells were double transfected 54h prior to plating in matrigel-covered chambers; mock transfected and not transfected cells were used as control. The cells were seeded on matrigel-covered membrane at 45k per insert in 5% FBS-DMEM. The cultures were placed in a 37°C humidified incubator with 5% CO_2. After 18h, the inserts were washed with PBS, had their inside cleaned with a cotton swab, and were placed in ice-cold methanol for 20 minutes to fix the cells that had migrated. The membranes were then cut out from the Transwell® inserts and mounted using VECTASHIELD Antifade Mounting Medium with DAPI (Vector Laboratories). Cell images were taken within the five independent fields (bottom, top, left, right side, and a center) of each specimen, using a fluorescence microscope (Leica DM4000B, 5× objective). Numbers of migrating cells' nuclei were counted using ImageJ software. Experiments were performed in duplicates six times in total. Statistical analysis was performed using GraphPad Prism software. The groups were compared using Wilcoxon test and differences considered significant when *P < 0.05.

REST-Chromatin immunoprecipitation

U87-IDHwt and U87-IDH1mut cells were plated at 10 cm plates, and the following day the cells were trypsinized, centrifuged, resuspended in PBS and fixed with 1% formaldehyde for 10 minutes. The cells were lysed and chromatin was isolated and fragmented by sonication (Covaris). Fragmented chromatin was loaded onto REST antibody (Millipore) or IgG (Millipore) - coated agarose beads (Invitrogen). Immunoprecipitated complexes were eluted and DNA was purified using DNA Clean&Concentrator kit (Zymo Research).

ChIP sequencing

DNA libraries for chromatin immunoprecipitation sequencing were prepared using QIAseq Ultra Low Input Library Kit (QIAGEN, Hilden, Germany) for two independent REST-ChIP experiments. Briefly, DNA was end-repaired, adenosines were added to the 3′ ends of dsDNA and adapters were ligated (adapters from NEB, Ipswich, MA, USA). Following the adapter ligation, uracil was digested by USER enzyme from NEB (Ipswich, MA, USA) in a loop structure of the adapter. Adapters containing DNA fragments were amplified by PCR using NEB starters (Ipswich MA, USA). Library quality evaluation was done with Agilent 2100 Bioanalyzer using the Agilent DNA High Sensitivity chip (Agilent Technologies, Ltd.). Quantification and quality evaluation of obtained samples were done using Nanodrop spectrophotometer (Thermo Scientific, NanoDrop products, Wilmington, USA), Quantus fluorometer (Promega Corporation, Madison, USA) and 2100 Bioanalyzer (Agilent

Technologies, Santa Clara, USA). The average length of the DNA fragments in the library was 300 bp. The libraries were run in the rapid run flow cell and were single-end sequenced (65 bp) on HiSeq 1500 (Illumina, San Diego, CA 92122 USA).

RNA sequencing

Total RNA was obtained from 3 passages of each U87-WT (ATCC HTB-14 IDH-WT) and U87-MUT (ATCC HTB-14IG) that were either not treated, control- or REST-siRNA transfected (Dharmacon, Lonza, Invitrogen). 500 ng of RNA was used for cDNA synthesis for transcriptome sequencing. mRNA sequencing libraries were prepared using KAPA Stranded mRNAseq Kit according to the manufacturer's protocol. Briefly, mRNA molecules were enriched from 500 ng of total RNA using poly-T oligo-attached magnetic beads (Kapa Biosystems, MA, USA). The first-strand cDNA was synthesized using a reverse transcriptase. Second cDNA synthesis was performed to generate double-stranded cDNA (dsDNA). Then, the adapter was ligated and the loop structure of the adapter was cut by USER enzyme (NEB, Ipswich, MA, USA). Amplification of obtained dsDNA fragments containing the adapters was performed using NEB starters (Ipswich, MA, USA). Quality control of obtained libraries was done using Agilent Bioanalyzer with High Sensitivity DNA Kit (Agilent Technologies, Palo Alto, CA, USA). Quantification of the libraries was done using Quantus Fluorometer and QuantiFluor Double Stranded DNA System (Promega, Madison, Wisconsin, USA). The libraries were run in the rapid run flow cell and were paired-end sequenced (2×76bp) on HiSeq 1500 (Illumina, San Diego, CA 92122 USA).

Glioma Atlas DNA methylation

DNA raw methylation data were kindly provided by the Authors of the Glioma Atlas. The data were processed with CytoMeth tool to obtain DNA methylation level expressed as beta value (β value) in a single nucleotide resolution.

Glioma Atlas RNA-seq data

RNA-seq raw data were kindly provided by the Authors of the Glioma Atlas. Following the recommendations, two normalization procedures were considered (10.1186/1471-2105-12-480): (i) within-lane to adjust for GC-content and gene-length; (ii) between-lane, both implemented in EDASeq 3.8 R package (10.1186/1471-2105-12-480). The normalized gene expressions were used to investigate correlation of DNA methylation level with gene expression.

DiffMeth module description

DiffMeth is a module that identifies statistically significant differences in methylation level of the given DNA regions among defined groups of samples. The input provided to this automatic analysis consisted of:

- DNA regions of interest defined in a standard bed file (chromosome, starting position, ending position, name of the region, name of the gene, strand).
- A set of standard bed files resulting from CytoMeth processing, containing cytosine methylation levels expressed as beta values for specific cytosine position on a given chromosome for a given sample. Each sample was defined by a separate bed file.

- A csv file defining the sample set, which contained methylation file name, sample name/ID, sample group (eg various types of cancer to be compared), ignore flag.
- Diffmeth input parameters defined in yaml file.

The first step of the analysis (significance criterion) is based on a standard chi2 statistical test where all groups are compared to each other (pair by pair) to discover possible differences between two groups out of *n* provided. Chi2 test compares distribution of beta values that belong to one of the following ranges: [0.0-0.2], [0.2-0.6], [0.6-1.0] for a given region, two compared groups and CG context. Finally in this step p-value is calculated (corrected by FDR). The second step (significance criterion) is based on Kruskal-Wallis statistical test applied on all groups at once similarly as before: for a given region and CG context and p-values corrected by FDR. The final interesting differential regions can be selected by intersection of results from both criteria where p-value<0.05.

QUANTIFICATION AND STATISTICAL ANALYSIS

Cell based assays

Quantitative PCR (qRT-PCR)

Data were obtained in 4 independent experiments. Statistical significance of comparisons between the groups was calculated in GraphPad Prism v. 9.1.2 (GraphPad Software, LCC). P values were considered significant when *P < 0.05 (Mann-Whitney test).

Western Blotting

Data were obtained in 4 independent experiments. REST band intensities were normalized to GAPDH band intensities for each blot. Statistical significance of comparisons between groups was calculated in GraphPad Prism v. 9.1.2 (GraphPad Software, LCC). P values were considered significant when *P < 0.05 (column statistics t-test).

PrestoBlueTM Cell Viability assay

Data were obtained in 3 independent experiments and analyzed in GraphPad Prism using Wilcoxon matched-pairs signed rank test, two-tailed. For each timepoint, mock transfected cells viability was normalized to 100%.

Matrigel Invasion assay

Numbers of migrating cells' nuclei were counted using ImageJ software. Experiments were performed in duplicates six times in total. Statistical analysis was performed using GraphPad Prism software. The groups were compared using Wilcoxon test and differences considered significant when *P < 0.05.

High-throughput analyses

Survival analyses

TCGA transcriptomic data (from both the LGG and GBM TCGA transcriptome datasets) were used to conduct four distinct survival studies, in which the patients were stratified into two

subgroups based on REST expression level (high REST mRNA and low REST mRNA);: the first one considered GBM patients with IDH-WT phenotype; the second one considered separate cohorts of GBMs and LGGs and (WHO II/III) patients harboring IDH1/2 mutations; the third one included patients with all glioma grades; and the fourth one that included LGG patients with wild-type IDH genes. Survival and survminer R libraries were used in the survival analyses and censored patients were included. To support the association between REST expression levels and patient survival, Kaplan-Meier estimators and the log-rank test were calculated.

U87 cell line IDH-phenotype cross validation with TCGA glioma data

In order to validate the U87 IDH-phenotype model, gene expression differences between U87-WT and its isogenic U87-MUT cell line were compared to the IDH-phenotype in the TCGA glioma transcriptomes dataset. First, log2 fold change (log2 FC) values of differentially expressed genes (DEGs) between U87-WT and U87-MUT were compared to log2 FC values from TCGA LGG IDH-MUT (defined in TCGA as a mutation in *IDH1/2*) vs IDH-WT comparison. To validate the relevance of overlap of DEGs with the same direction of change in U87 and TCGA tumors MUT-WT comparisons, a bootstrapping technique (sampling 10000 times) was applied. Next, tumor samples from the TCGA repository (WHO grades II-IV, GBM + LGG set) were divided into IDH-WT (n=86) and IDH-MUT (n=365). Two differential analyses were carried out: 1) LGG IDH-WT vs LGG IDH-MUT and U87 IDH-WT vs U87 IDH-MUT. REACTOME Pathways enrichment analysis was performed on a selection of the most significantly changed DEGs (FDR<0.01) obtained from differentially up- (log2 FC>0) and down-regulated (log FC <0) genes, separately.

Transcriptomics data

RNA sequencing reads were aligned to the human genome with the STAR algorithm (https://www.ncbi.nlm.nih.gov/pmc/articles/PMC3530905/), a fast gap-aware mapper. Then, gene counts were obtained by featurecounts (10.1093/nar/gkz114) using human genome annotations. The counts were then imported to R and processed by DESeq2 (https://doi.org/10.1186/s13059-014-0550-8). The counts were normalized for gene length and library size and statistical analysis was done by DESeq2 for the following comparisons: IDH-MUT/WT isogenic cell lines, siREST/siCTRL treated IDH-MUT cell line and siREST/siCTRL treated IDH-WT cell line. Gene pathways analysis (KEGG, Gene Ontology, REACTOME) were performed using clusterProfiler R library (10.1089/omi.2011.0118). Gene Ontology Biological Processes (GO BP) analysis for DEGs arising from REST knockdown in U87-WT and U87-MUT was done separately for down- (log2 foldchange <0 and adjusted p-value<0.05) and up-regulated (log2 foldchange >0 and adjusted p-value<0.05) genes from a pool of IDH-MUT and IDH-WT DEGs.

REST ChIP-seq data processing

Two replicates for U87-WT and two for U87-MUT cell lines were immunoprecipitated with REST antibody and processed for DNA sequencing. Input DNA was sequenced as a control. Sequencing libraries were generated using the QIAseq Ultra Low Input Library Kit, Qiagen, Cat No./ID: 180492. Template amplification and cluster generation were performed using the TruSeq SBS Kit v3 and 50 nucleotides were sequenced with Illumina HiSeq 1500. After quality filtering (average Phred >30) and removal of duplicates, reads were mapped to the human genome (hg38) with the BWA MEM tool. Samtools view was used to filter best quality reads

(-q 20 and -F 256 flags) before peak calling. The peaks were called using the Model-based Analysis of ChIP-Seq (MACS2) algorithm (Feng et al. 2012) with default parameters; peaks with q-value < 0.01 were considered in the analysis. Peaks were annotated to genes using ChIPseeker (10.1093/bioinformatics/btv145.) and subsequent pathway analysis was performed with clusterProfiler (10.1089/omi.2011.0118). The raw ChIP-seq data were deposited in the NCBI GEO database: GSE174308.
For further analysis, the consensus REST ChIP-seq peaks were generated as follows: the datasets for experiment repeat 1 and 2 were intersected for each U87-WT and U87-MUT datasets, separately. The resulting peaks (present in both repeats of the experiment) were then limited to the length of 200 bp (±100 bp from the peak summit, that was defined as a middle point of the obtained peak) for further TF motifs and DNA methylation analysis. Peaks were centered and limited to 200 bp in order to have a more consistent and homogenous set of observations. The resulting consensus peaks for U87-WT and U87-MUT were then intersected again to yield peaks common to both U87-WT and U87-MUT, peaks were also subtracted from each other to receive peaks specific to U87-WT and specific to U87-MUT.

Defining REST-activated and REST-repressed genes

The putative REST target genes were defined as those with a REST-ChIP-seq peak within a promoter (10.1093/bioinformatics/btv145.) in at least one of the ChIP-seq experiment repeats in either U87-WT or U87-MUT. Annotation of REST-ChIP-seq peaks to promoter genes was performed with ChIPseeker. REST ChIP-seq peak U87-WT and U87-MUT datasets for both sets were pooled. The peak summits were assigned as the middle point of each existing peak, and 200 bp peak sequences were generated covering 100 bp upstream and downstream of the summit. Next, genes defined as REST targets by ChIPseeker based on U87-WT and U87-MUT ChIP-seq experiments were correlated (Pearson's correlation) with REST expression levels in the joined LGG/GBM TCGA transcriptome dataset. Genes that had significant positive correlation (correlation coefficient >0.15, Bonferroni corrected p-value<0.0001) of their mRNA level with that of REST were defined as REST-activated, while these having significant inverse correlation (correlation coefficient < -0.15, Bonferroni corrected p-value<0.0001) were defined as REST-repressed.

Intersection of REST knockdown and REST ChIP-seq data

Gene targets of REST defined by REST ChIP-seq (588 activated, 981 repressed) were intersected with REST gene targets as defined by REST knockdown. The REST ChIP-seq gene targets that had decreased expression upon REST knockdown were defined as REST activation targets, while those that had increased expression upon REST silencing were defined as REST repression targets. Separately, Gene Ontology Biological Process (GO BP) analysis was performed for both groups using clusterProfiler and GO BP database.

Intersection of REST ChIP-seq peaks with ENCODE database

REST ChIP-seq peaks (peak summit ± 100bp) were submitted to the Enrichr tool (https://maayanlab.cloud/Enrichr/) in order to predict transcription factors binding sites deposited in ENCODE.

A position weight matrix (PWM) analysis

To identify the transcription factors (TF) motifs within the REST ChIP-seq peaks a PWM analysis was performed on two datasets. The first dataset consisted of the sequences assigned to REST-activated (n=588) and REST-repressed genes (n=981). The second dataset contained sequences stratified according to the IDH gene mutation status (WT-specific n=1007, MUT-specific n=114, peaks common between both n=2647).
The 200 bp peak sequences were used as an input for known motif search using the PWMEnrich Bioconductor R package [R-PWMEnrich] and open-access HOCOMOCO database (see Key Resources Table) with 14 additional REST matrices obtained from ENCODE. To identify TF motifs, 10765 selected promoters active in tumor samples were used as a background (dataset derived from Stepniak et al, 2021) to proceed lognormal distribution background correction. Only these motifs for which the p-value of motif enrichment was lower than 0.001 were selected for further analysis. Due to the notable difference in the number of sequences between IDH-WT (n = 1007) and IDH-MUT (n = 114), ten draws of 114 sequences from the IDH-WT sequence pool were made. A separate analysis of the search for motifs using PWMEnrich R package was performed on each of these ten sets. In parallel, the same analysis was performed on the set of all the sequences characteristic for IDH-WT (n = 1007). For further IDH status analysis, motifs common between the sum of TF motifs from ten draws and the motifs identified on the set of all available sequences were selected. To identify transcription factor binding sites (TFBS), defined as each occurrence of the motif in the sequence, an online FIMO tool from MEME Suite 5.0.1 was used (see Key Resources Table). FIMO scans sequences as double stranded and matches motifs to both forward and backward strands. The p-value threshold for the FIMO output was set to 0.001.
For further analysis, only the TFBS with the q-value lower than 0.05 were considered (correction done using Benjamini and Hochberg procedure). The TF motifs specific for these TFBS were grouped by sequence using the STAMP website tool (see Key Resources Table). To compare motif sequences during grouping, the Pearson correlation coefficient was used. As an aligning method, the ungapped Smith-Waterman followed by an iterative refinement multiple alignment strategy was used. Finally, the UPGMA tree-building algorithm was used. An enrichment analysis was done using Fisher's exact test with an FDR correction. Transcription factor families were identified based on the HOCOMOCO database, which uses data from the Classification of Transcription Factors in Mammalia database (see Key Resources Table). The CentriMo tool from MEME Suite 5.4.1 allows us to determine the position distribution of each motif on the sequences, and then check the local enrichment of the given sequences with selected motifs and calculate the static significance of the result using the binomial test (see Key Resources Table). The analysis was performed for the entire sequence length assuming E-value threshold ≤ 10.

REST peaks hierarchical clustering

To cluster by similarity the peaks with detected REST and KAISO motifs, each peak was changed into a binary vector, where a REST or KAISO motif was assigned value=1 if present in a peak or value=0 if absent in a peak. Such vectors were used as the input into hierarchical clustering performed with the Heatmap function from the ComplexHeatmap R package, using the default setting. Grouping was done by rows.

DNA methylation data analysis

Discretization of β-value

DNA methylation ranges from 0 to 1. It was discretized into three classes: low/hypomethylation [0-0.2], medium (0.2-0.6] and high/hypermethylation (0.6-1].

Selecting regions with differential DNA methylation

DNA methylation analysis was performed on the two region types: peaks that cover a sequence of ±100 bp from the peak summit, and TF site motifs that mean a range of DNA sequence where the presence of a TF motif was statistically confirmed.
We used the DiffMeth module with false discovery rate correction (FDR) for multiple testing, to identify regions with significantly different DNA methylation patterns. The results with FDR<0.05 were considered statistically significant.
In the context of TF motifs differential analysis, where the motifs frequently overlap with each other, a repeated selection of the same cytosine for a single TF data set was prevented. If a cytosine was located within multiple motifs of a single TF due to the motifs overlapping, its beta value was counted only once. When a cytosine was within motifs of different TFs (REST or KAISO), its beta value (β) was counted separately for motifs of a TF.

Comparison of DNA methylation between classes

To compare the number of low, medium, and high-methylated cytosines between the classes we used the Chi-Square test. To compare DNA methylation (β-value) between two classes we used the Wilcoxon rank sum test, and for more than two classes we used the Kruskal-Wallis test. The results with p<0.05 were considered significant.

Neftel et al 2019 data analysis

Data were analyzed in R, expression of a certain gene was correlated (Pearson's correlation) with certain cell states as defined by Neftel et al 2019 including NPC-like1, NPC-like2, MES-like1, MES-like2, OPC-like, AC-like, G1S and G2M.

Availability of data and materials

GSE174308 - REST transcription factor holds the balance between the invasion and cell differentiation in IDH-mutant and IDH-wild type gliomas

EGAD00001008986 - Glioma specimens of both IDH-MUT and IDH-WT REST ChIPseq data

Abbreviations

2HG - 2-hydroxyglutarate
5mC - 5-methylcytosine
α-KG - α-ketoglutarate
AC-like - astrocyte-like
ChIP-seq - chromatin immunoprecipitation-sequencing
coREST – corepressor REST
CpG - cytosine phosphate guanine

dDEG - decreased DEG (a gene differentially expressed in IDH-WT and IDH-MUT that had a lower fold change in siREST-transfected cells than in siCTRL transfected cells)
DEG - differentially expressed gene
ECM - extracellular matrix
ENCODE - The Encyclopedia of DNA Elements
GBM - glioblastoma, WHO grade IV
GII - WHO grade II
GIII - WHO grade III
GIV - WHO grade IV
GO - Gene Ontology
GSC – glioma stem cell
HOCOMOCO - HOmo sapiens COmprehensive MOdel COllection
iDEG - increased DEG (genes differentially expressed in IDH-WT and IDH-MUT that had a higher fold change in siREST-transfected cells than in siCTRL transfected cells)
IDH (1/2)- isocitrate dehydrogenase (1 or 2)
IDH-MUT - mutated isocitrate dehydrogenase 1 or 2
IDH-WT - IDH wild type samples (neither IDH1 nor IDH2 were mutated)
LGG - lower grade gliomas, WHO grades II and III
MES-like - mesenchymal-like
NB - normal brain
NPC – neural progenitor cell
OPC - oligodendrocyte-progenitor cell
PNET - primitive neuroepithelial tumors
PWM - position weighted matrix
RE1 - repressor element-1
REST - repressor element-1-silencing transcription factor / RE1 silencing transcription factor/neural-restrictive silencing factor (also known as neuron-restrictive silencer factor NRSF)
REST4 - repressor element-1 silencing transcription factor-4
siRNA – short interfering RNA
TCGA - The Cancer Genome Atlas
ZBTB33 - Zinc Finger And BTB Domain Containing 33 transcription factor (also known as KAISO)

References

Abramovitz, L., Shapira, T., Ben-Dror, I., Dror, V., Granot, L., Rousso, T., Landoy, E., Blau, L., Thiel, G., and Vardimon, L. (2008). Dual Role of NRSF/REST in Activation and Repression of the Glucocorticoid Response *. Journal of Biological Chemistry *283*, 110–119. https://doi.org/10.1074/jbc.M707366200.

Andrysik, Z., Kim, J., Tan, A.C., and Espinosa, J.M. (2013). A genetic screen identifies TCF3/E2A and TRIAP1 as pathway-specific regulators of the cellular response to p53 activation. Cell Rep *3*, 1346–1354. https://doi.org/10.1016/j.celrep.2013.04.014.

Ballas, N., Grunseich, C., Lu, D.D., Speh, J.C., and Mandel, G. (2005). REST and its corepressors mediate plasticity of neuronal gene chromatin throughout neurogenesis. Cell *121*, 645–657. https://doi.org/10.1016/j.cell.2005.03.013.

Blattler, A., Yao, L., Wang, Y., Ye, Z., Jin, V.X., and Farnham, P.J. (2013). ZBTB33 binds unmethylated regions of the genome associated with actively expressed genes. Epigenetics & Chromatin *6*, 13. https://doi.org/10.1186/1756-8935-6-13.

Callegari, K., Maegawa, S., Bravo-Alegria, J., and Gopalakrishnan, V. (2018). Pharmacological inhibition of LSD1 activity blocks REST-dependent medulloblastoma cell migration. Cell Commun Signal *16*, 60. https://doi.org/10.1186/s12964-018-0275-5.

Chan, J.Y.H., Chen, W.-C., Lee, H.-Y., Chang, T.-J., and Chan, S.H.H. (1999). Phosphorylation of transcription factor CREB mediates c-fos induction elicited by sustained hypertension in rat nucleus tractus solitarii. Neuroscience *88*, 1199–1212. https://doi.org/10.1016/S0306-4522(98)00273-5.

Conti, L., Crisafulli, L., Caldera, V., Tortoreto, M., Brilli, E., Conforti, P., Zunino, F., Magrassi, L., Schiffer, D., and Cattaneo, E. (2012). REST Controls Self-Renewal and Tumorigenic Competence of Human Glioblastoma Cells. PLOS ONE *7*, e38486. https://doi.org/10.1371/journal.pone.0038486.

Dabrowski, M.J., Draminski, M., Diamanti, K., Stepniak, K., Mozolewska, M.A., Teisseyre, P., Koronacki, J., Komorowski, J., Kaminska, B., and Wojtas, B. (2018). Unveiling new interdependencies between significant DNA methylation sites, gene expression profiles and glioma patients survival. Sci Rep *8*, 4390. https://doi.org/10.1038/s41598-018-22829-1.

Dang, L., White, D.W., Gross, S., Bennett, B.D., Bittinger, M.A., Driggers, E.M., Fantin, V.R., Jang, H.G., Jin, S., Keenan, M.C., et al. (2009). Cancer-associated IDH1 mutations produce 2-hydroxyglutarate. Nature *462*, 739–744. https://doi.org/10.1038/nature08617.

Daniel, J.M., Spring, C.M., Crawford, H.C., Reynolds, A.B., and Baig, A. (2002). The p120ctn-binding partner Kaiso is a bi-modal DNA-binding protein that recognizes both a sequence-specific consensus and methylated CpG dinucleotides. Nucleic Acids Res *30*, 2911–2919. .

Darieva, Z., Clancy, A., Bulmer, R., Williams, E., Pic-Taylor, A., Morgan, B.A., and Sharrocks, A.D. (2010). A Competitive Transcription Factor Binding Mechanism Determines the Timing of Late Cell Cycle-Dependent Gene Expression. Mol Cell *38*, 29–40. https://doi.org/10.1016/j.molcel.2010.02.030.

Davis, R.L., and Turner, D.L. (2001). Vertebrate hairy and Enhancer of split related proteins: transcriptional repressors regulating cellular differentiation and embryonic patterning. Oncogene *20*, 8342–8357. https://doi.org/10.1038/sj.onc.1205094.

Flavahan, W.A., Drier, Y., Liau, B.B., Gillespie, S.M., Venteicher, A.S., Stemmer-Rachamimov, A.O., Suvà, M.L., and Bernstein, B.E. (2016). Insulator dysfunction and oncogene activation in IDH mutant gliomas. Nature *529*, 110–114. https://doi.org/10.1038/nature16490.

Grant, C.E., Bailey, T.L., and Noble, W.S. (2011). FIMO: scanning for occurrences of a given motif. Bioinformatics *27*, 1017–1018. https://doi.org/10.1093/bioinformatics/btr064.

Gurdon, J.B., Javed, K., Vodnala, M., and Garrett, N. (2020). Long-term association of a transcription factor with its chromatin binding site can stabilize gene expression and cell fate commitment. Proceedings of the National Academy of Sciences *117*, 15075–15084. https://doi.org/10.1073/pnas.2000467117.

Huang, J., Yu, J., Tu, L., Huang, N., Li, H., and Luo, Y. (2019). Isocitrate Dehydrogenase Mutations in Glioma: From Basic Discovery to Therapeutics Development. Front Oncol *9*, 506. https://doi.org/10.3389/fonc.2019.00506.

J. Dabrowski, M., and Wojtas, B. (2019). Global DNA Methylation Patterns in Human Gliomas and Their Interplay with Other Epigenetic Modifications. International Journal of Molecular Sciences *20*, 3478. https://doi.org/10.3390/ijms20143478.

Kamal, M.M., Sathyan, P., Singh, S.K., Zinn, P.O., Marisetty, A.L., Liang, S., Gumin, J., El-Mesallamy, H.O., Suki, D., Colman, H., et al. (2012). REST regulates oncogenic properties of glioblastoma stem cells. Stem Cells *30*, 405–414. https://doi.org/10.1002/stem.1020.

Lee, M.G., Wynder, C., Cooch, N., and Shiekhattar, R. (2005). An essential role for CoREST in nucleosomal histone 3 lysine 4 demethylation. Nature *437*, 432–435. https://doi.org/10.1038/nature04021.

Lee, N., Park, S.J., Haddad, G., Kim, D.-K., Park, S.-M., Park, S.K., and Choi, K.Y. (2016). Interactomic analysis of REST/NRSF and implications of its functional links with the transcription suppressor TRIM28 during neuronal differentiation. Sci Rep *6*, 39049. https://doi.org/10.1038/srep39049.

Liang, J., Meng, Q., Zhao, W., Tong, P., Li, P., Zhao, Y., Zhao, X., and Li, H. (2016). An expression based REST signature predicts patient survival and therapeutic response for glioblastoma multiforme. Sci Rep *6*, 34556. https://doi.org/10.1038/srep34556.

van Lith, S.A.M., Molenaar, R., van Noorden, C.J.F., and Leenders, W.P.J. (2014). Tumor cells in search for glutamate: an alternative explanation for increased invasiveness of IDH1 mutant gliomas. Neuro Oncol *16*, 1669–1670. https://doi.org/10.1093/neuonc/nou152.

Loveys, D.A., Streiff, M.B., and Kato, G.J. (1996). E2A Basic-Helix-Loop-Helix Transcription Factors are Negatively Regulated by Serum Growth Factors and by the Id3 Protein. Nucleic Acids Research *24*, 2813–2820. https://doi.org/10.1093/nar/24.14.2813.

Mandel, G., Fiondella, C.G., Covey, M.V., Lu, D.D., LoTurco, J.J., and Ballas, N. (2011). Repressor element 1 silencing transcription factor (REST) controls radial migration and temporal neuronal specification during neocortical development. Proceedings of the National Academy of Sciences *108*, 16789–16794. https://doi.org/10.1073/pnas.1113486108.

Nechiporuk, T., McGann, J., Mullendorff, K., Hsieh, J., Wurst, W., Floss, T., and Mandel, G. (2016). The REST remodeling complex protects genomic integrity during embryonic neurogenesis. ELife *5*, e09584. https://doi.org/10.7554/eLife.09584.

Neftel, C., Laffy, J., Filbin, M.G., Hara, T., Shore, M.E., Rahme, G.J., Richman, A.R., Silverbush, D., Shaw, M.L., Hebert, C.M., et al. (2019). An integrative model of cellular states, plasticity and genetics for glioblastoma. Cell *178*, 835-849.e21. https://doi.org/10.1016/j.cell.2019.06.024.

Noh, K.-M., Hwang, J.-Y., Follenzi, A., Athanasiadou, R., Miyawaki, T., Greally, J.M., Bennett, M.V.L., and Zukin, R.S. (2012). Repressor element-1 silencing transcription factor (REST)-dependent epigenetic remodeling is critical to ischemia-induced neuronal death. Proc Natl Acad Sci U S A *109*, E962-971. https://doi.org/10.1073/pnas.1121568109.

Oikawa, T., and Yamada, T. (2003). Molecular biology of the Ets family of transcription factors. Gene *303*, 11–34. https://doi.org/10.1016/s0378-1119(02)01156-3.

Pientka, F.K., Hu, J., Schindler, S.G., Brix, B., Thiel, A., Jöhren, O., Fandrey, J., Berchner-Pfannschmidt, U., and Depping, R. (2012). Oxygen sensing by the prolyl-4-hydroxylase PHD2 within the nuclear compartment and the influence of compartmentalisation on HIF-1 signalling. J Cell Sci *125*, 5168–5176. https://doi.org/10.1242/jcs.109041.

Pierre, C.C., Hercules, S.M., Yates, C., and Daniel, J.M. (2019). Dancing from bottoms up - Roles of the POZ-ZF transcription factor Kaiso in Cancer. Biochim Biophys Acta Rev Cancer *1871*, 64–74. https://doi.org/10.1016/j.bbcan.2018.10.005.

Pierre, C.C., Hercules, S.M., Yates, C., and Daniel, J.M. (2019b). Dancing from bottoms up - Roles of the POZ-ZF transcription factor Kaiso in Cancer. Biochim Biophys Acta Rev Cancer *1871*, 64–74. https://doi.org/10.1016/j.bbcan.2018.10.005.

Pilotto, S., Speranzini, V., Tortorici, M., Durand, D., Fish, A., Valente, S., Forneris, F., Mai, A., Sixma, T.K., Vachette, P., et al. (2015). Interplay among nucleosomal DNA, histone tails, and corepressor CoREST underlies LSD1-mediated H3 demethylation. Proc Natl Acad Sci U S A *112*, 2752–2757. https://doi.org/10.1073/pnas.1419468112.

Prokhortchouk, A., Hendrich, B., Jørgensen, H., Ruzov, A., Wilm, M., Georgiev, G., Bird, A., and Prokhortchouk, E. (2001). The p120 catenin partner Kaiso is a DNA methylation-dependent transcriptional repressor. Genes Dev *15*, 1613–1618. https://doi.org/10.1101/gad.198501.

Rodríguez-Seoane, C., Ramos, A., Korth, C., and Requena, J.R. (2015). DISC1 regulates expression of the neurotrophin VGF through the PI3K/AKT/CREB pathway. J Neurochem *135*, 598–605. https://doi.org/10.1111/jnc.13258.

Stadler, M.B., Murr, R., Burger, L., Ivanek, R., Lienert, F., Schöler, A., Nimwegen, E. van, Wirbelauer, C., Oakeley, E.J., Gaidatzis, D., et al. (2011). DNA-binding factors shape the mouse methylome at distal regulatory regions. Nature *480*, 490–495. https://doi.org/10.1038/nature10716.

Stępniak, K., Machnicka, M.A., Mieczkowski, J., Macioszek, A., Wojtaś, B., Gielniewski, B., Poleszak, K., Perycz, M., Król, S.K., Guzik, R., et al. (2021). Mapping chromatin accessibility and active regulatory elements reveals pathological mechanisms in human gliomas. Nat Commun *12*, 3621. https://doi.org/10.1038/s41467-021-23922-2.

Sussman, C.R., Davies, J.E., and Miller, R.H. (2002). Extracellular and intracellular regulation of oligodendrocyte development: roles of Sonic hedgehog and expression of E proteins. Glia *40*, 55–64. https://doi.org/10.1002/glia.10114.

Tang, Y., Urs, S., and Liaw, L. (2008). Hairy-related transcription factors inhibit Notch-induced smooth muscle alpha-actin expression by interfering with Notch intracellular domain/CBF-1 complex interaction with the CBF-1-binding site. Circ Res *102*, 661–668. https://doi.org/10.1161/CIRCRESAHA.107.165134.

Taylor, P., Fangusaro, J., Rajaram, V., Goldman, S., Helenowski, I.B., MacDonald, T., Hasselblatt, M., Riedemann, L., Laureano, A., Cooper, L., et al. (2012). REST is a novel prognostic factor and therapeutic target for medulloblastoma. Mol Cancer Ther *11*, 1713–1723. https://doi.org/10.1158/1535-7163.MCT-11-0990.

Taylor, P., Fangusaro, J., Rajaram, V., Goldman, S., Helenowski, I.B., MacDonald, T., Hasselblatt, M., Riedemann, L., Laureano, A., Cooper, L., et al. (2012b). REST is a novel prognostic factor and therapeutic target for medulloblastoma. Mol Cancer Ther *11*, 1713–1723. https://doi.org/10.1158/1535-7163.MCT-11-0990.

Turcan, S., Makarov, V., Taranda, J., Wang, Y., Fabius, A.W.M., Wu, W., Zheng, Y., El-Amine, N., Haddock, S., Nanjangud, G., et al. (2018). Mutant-IDH1-dependent chromatin state reprogramming, reversibility, and persistence. Nature Genetics *50*, 62–72. https://doi.org/10.1038/s41588-017-0001-z.

Verhaak, R.G.W., Hoadley, K.A., Purdom, E., Wang, V., Qi, Y., Wilkerson, M.D., Miller, C.R., Ding, L., Golub, T., Mesirov, J.P., et al. (2010). An integrated genomic analysis identifies clinically relevant subtypes of glioblastoma characterized by abnormalities in PDGFRA, IDH1, EGFR and NF1. Cancer Cell *17*, 98. https://doi.org/10.1016/j.ccr.2009.12.020.

Wagoner, M.P., and Roopra, A. (2012). A REST derived gene signature stratifies glioblastomas into chemotherapy resistant and responsive disease. BMC Genomics *13*, 686. https://doi.org/10.1186/1471-2164-13-686.

Xu, W., Yang, H., Liu, Y., Yang, Y., Wang, P., Kim, S.-H., Ito, S., Yang, C., Wang, P., Xiao, M.-T., et al. (2011). Oncometabolite 2-Hydroxyglutarate Is a Competitive Inhibitor of α-Ketoglutarate-Dependent Dioxygenases. Cancer Cell *19*, 17–30. https://doi.org/10.1016/j.ccr.2010.12.014.

Yu, T., Lin, Y., Xu, Y., Dou, Y., Wang, F., Quan, H., Zhao, Y., and Liu, X. (2020). Repressor Element 1 Silencing Transcription Factor (REST) Governs Microglia-Like BV2 Cell Migration via Progranulin (PGRN). Neural Plasticity *2020*, e8855822. https://doi.org/10.1155/2020/8855822.

Zabet, N.R., and Adryan, B. (2013). The effects of transcription factor competition on gene regulation. Frontiers in Genetics *4*. .

Zhang, D., Li, Y., Wang, R., Li, Y., Shi, P., Kan, Z., and Pang, X. (2016). Inhibition of REST Suppresses Proliferation and Migration in Glioblastoma Cells. Int J Mol Sci *17*, E664. https://doi.org/10.3390/ijms17050664.

Zhang, D., Wu, B., Wang, P., Wang, Y., Lu, P., Nechiporuk, T., Floss, T., Greally, J.M., Zheng, D., and Zhou, B. (2017). Non-CpG methylation by DNMT3B facilitates REST binding and gene silencing in developing mouse hearts. Nucleic Acids Res *45*, 3102–3115. https://doi.org/10.1093/nar/gkw1258.

Zhao, H., Zhao, C., Li, H., Zhang, D., and Liu, G. (2019). E2A attenuates tumor-initiating capacity of colorectal cancer cells via the Wnt/beta-catenin pathway. Journal of Experimental & Clinical Cancer Research *38*, 276. https://doi.org/10.1186/s13046-019-1261-5.

Acknowledgments

We would like to thank Beata Kaza, Sylwia Katarzyna Król, Natalia Ochocka, Iwona Ciechomska, Kamil Wojnicki, Katarzyna Poleszak, Paulina Szadkowska and Aleksandra Ellert-Miklaszewska for their help in the laboratory work and helpful comments and suggestions. We would like to thank to Anna Malik and Beata Konikowska for critical manuscript draft revision.

Funding

Studies were supported by the Foundation for Polish Science TEAM-TECH Core Facility project “NGS platform for comprehensive diagnostics and personalized therapy in neuro-oncology” and NCN Symfonia 3 grant nr DEC-2015/16/W/NZ2/00314. The use of CePT infrastructure, financed by the European Union, The European Regional Development Fund within the Operational Program “Innovative economy” for 2007–2013, is highly appreciated.

Author information

Contributions

MP, BG, KS performed wet lab experiments and sequencing,
MP, BW, AJC, MJD, MJ, MDR analyzed data
MP, BW, AJC, MJ, MJD made the figures
BW, MP, BK, MJD designed the research
BW, MP, MJ, MJD, AJC, MDR, BK wrote the paper.
All the authors read and approved the final manuscript.

Corresponding authors

Correspondence to BW

Ethics declarations

Ethics approval and consent to participate

not applicable